AD-763 709

RESEARCH AND DEVELOPMENT ON LASER, SEMICONDUCTING AND
MAGNETIC MATERIALS

DAYTON UNIVERSITY

PREPARED FOR
AIR FORCE MATERIALS LABORATORY

JANU RY 1973

RESEARCH AND DEVELOPMENT ON

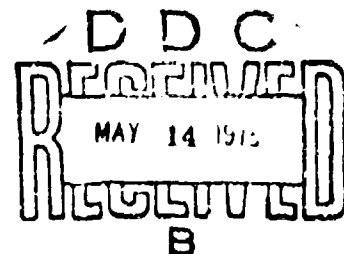# LASER, SEMICONDUCTING AND MAGNETIC MATERIALS

AD 763709

Dr. Perry P. Yaney
Mr. John A. Detrio
Dr. J. Michael O'Hare
Dr. Clark W. Searle
Dr. Rex L. Jones

University of Dayton
Research Institute
Dayton, Ohio 45469

TECHNICAL REPORT AFML-TR-73-52

April 1973

Approved for public release; distribution
unlimited

D D C

RECEIVED

MAY 14 1973

B

AIR FORCE MATERIALS LABORATORY

AIR FORCE SYSTEMS COMMAND

WRIGHT-PATTERSON AIR FORCE BASE, OHIO

NOTICE

When Government drawings, specifications, or othe   .a are used for
any purpose other than in connection with a definitely related Government
procurement operation, the United States Government thereby incurs no
responsibility nor any obligation whatsoever; and the fact that the Government
may have formulated, furnished, or in any way supplied the said drawings,
specifications, or other data, is not to be regarded by implication or
otherwise as in any manner licensing the holder or any other person or
corporation, or conveying any rights or permission to manufacture, use, or
sell any patented invention that may in any way be related thereto.

Copies of this report should not be returned unless return is required
by security considerations, contractual obligations, or notice on a specific
document.

DOCUMENT CONTROL DATA - R & D

(Security classification of title, body of abstract and indexing annotation must be entered when the overall report is classified)

1 ORIGINATING ACTIVITY (Corporate author)	2a. REPORT SECURITY CLASSIFICATION
University of Dayton Research Institute Dayton, Ohio 45469	UNCLASSIFIED
	2b. GROUP

3 REPORT TITLE

RESEARCH AND DEVELOPMENT ON LASER, SEMICONDUCTING AND MAGNETIC MATERIALS

4 DESCRIPTIVE NOTES (Type of report and inclusive dates)

Final Report (1 November 1970 to 1 December 1972)

5 AUTHOR(S) (First name, middle initial, last name)

Perry P. Yaney   Clark W. Searle
John A. Detrio   Rex L. Jones
J. Michael O'Hare

6 REPORT DATE	7a. TOTAL NO. OF PAGES	7b. NO. OF REFS
January 1973	87 88	60

8a CONTRACT OR GRANT NO	9a. ORIGINATOR'S REPORT NUMBER(S)
F33615-71-C01121	
b. PROJECT NO 7371	UDRI-TR-73-01
c.	9b. OTHER REPORT NO(S) (Any other numbers that may be assigned this report)
d.	

10 DISTRIBUTION STATEMENT

Approved for public release; distribution unlimited.

11 SUPPLEMENTARY NOTES	12 SPONSORING MILITARY ACTIVITY
	Air Force Materials Laboratory (LPE) Wright-Patterson AFB, Ohio 45433

13 ABSTRACT

A final report on the work accomplished during a two-year program on laser, semiconducting, and magnetic materials is presented. The laser materials studied included $YAlO_3$: Er^{3+}, SrF_2: (Gd^{3+}, Ce^{3+}), and CdF_2: (Gd^{3+}, Ce^{3+}). High-resolution optical spectroscopy and EPR studies were carried out.

Electrical characteristics of the insulating and semiconducting states of the doped CdF_2 system were studied and LED's were constructed using this system. Extensive theoretical and computational studies were carried out on the $YAlO_3$ and SrF_2 doped materials. An experimental facility for the evaluation of laser materials at the sponsor's site was begun. The pulsed Raman technique was developed.

Electrical and optical properties of ZnSe doped with Li, Cu, or Na as well as samples implanted with Zn and samples of ZnO hydrothermally grown with Li, CdS, or ZnS were studied. Also, measurements were made on radiation damaged Ge and Si. The intrinsic coercive force in multidomain single crystal (rare earth) Co_5 alloys were studied and a model describing the observed behavior is presented.

KEY WORDS	LINK A		LINK B		LINK C	
	ROLE	WT	ROLE	WT	ROLE	WT
Rare-earth ions						
Lasers						
Absorption spectra						
Fluorescence spectra						
Lifetimes						
$YA\ell O_3 : Er^{3+}$,						
$SrF_2 : (Gd^{3+} + Ce^{3+})$						
$CdF_2 : (Gd^{3+} + Ce^{3+})$,						
EPR						
Free-ion						
Crystal Field						
Intensities						
Ion-clustering						
Theoretical						
Experimental						
Computational						
LED						
Raman						
Semiconductor						
Hall effect						
Van der Pauw						
ZnSe						
ZnO						
CdS						
ZnS						
Implantation						
Hydrothermal growth						
Ge						
Si						
Radiation damage						
$SmCo_5$						
$NdCo_5$						
YCo_5						
Intrinsic coercive force						
Alloys						
Domain wall						
hysteresis						
Pinning sites						
Magnetic susceptability						
Relaxation						

RESEARCH AND DEVELOPMENT ON LASER, SEMICONDUCTING AND MAGNETIC MATERIALS

Dr. Perry P. Yaney
Mr. John A. Detrio
Dr. J. Michael O'Hare
Dr. Clark W. Searle
Dr. Rex L. Jones

FOREWORD

This report has been reviewed and is approved.

Major William Goldberg, USAF
Chief, Laser and Optical Materials Branch
Air Force Materials Laboratory

ABSTRACT

A final report on the work accomplished during a two-year program on laser, semiconducting, and magnetic materials is presented. The laser materials studied included $YAlO_3:Er^{3+}$, $SrF_2:(Gd^{3+}, Ce^{3+})$, and $CdF_2:(Gd^{3+}, Ce^{3+})$. High-resolution optical spectroscopy and EPR studies were carried out.

Electrical characteristics of the insulating and semiconducting states of the doped CdF_2 system were studied and LED's were constructed using this system. Extensive theoretical and computational studies were carried out on the $YAlO_3$ and SrF_2 doped materials. An experimental facility for the evaluation of laser materials at the sponsor's site was begun. The pulsed Raman technique was developed.

Electrical and optical properties of ZnSe doped with Li, Cu, or Na as well as samples implanted with Zn and samples of ZnO hydrothermally grown with Li, CdS, or ZnS were studied. Also, measurements were made on radiation damaged Ge and Si. The intrinsic coercive force in multidomain single crystal (rare earth) Co_5 alloys were studied and a model describing the observed behavior is presented.

TABLE OF CONTENTS

PART I: LASER MATERIALS STUDIES

PART II: ELECTRICAL AND OPTICAL PROPERTIES OF SEMICONDUCTING MATERIALS

TABLE OF CONTENTS (continued)

PART III: INTRINSIC COERCIVE FORCE IN MULTIDOMAIN
SINGLE CRYSTAL (RARE EARTH) Co_5 ALLOYS

LIST OF ILLUSTRATIONS

LIST OF TABLES

PART I

LASER MATERIALS STUDIES

Dr. Perry P. Yaney
Mr. John A. Detrio
Dr. J. Michael O'Hare
Department of Physics

INTRODUCTION

This part presents the work performed on laser materials and is divided into seven sections. Sections 1, 2, 3, 6, and 7 are in summary form. Details of the work described in these sections can be obtained from published papers or from preprints of papers in preparation obtainable from the authors. A complete listing of reports, presentations, and publications resulting from the work reported herein is given in Section 8.

SECTION 1

ANALYSES OF OPTICAL SPECTRA

1.1 Gd^{3+} in SrF_2

The fluorites, namely Ca, Sr, and BaF_2, have continued to provide a fruitful series of lattices to study the many processes and circumstances associated with a RE ion in a dielectric host. Of particular importance to the development of solid-state lasers is the question of line strengths, especially their calculation when the ion is in a given site symmetry. The large amount of experimental and calculational information available on Gd^{3+}, particularly in the C_{4v} site of SrF_2,[1] made this ion a convenient choice for line strength analyses. A selected review[1-4] of the energy level schemes of Gd^{3+} in various hosts is shown in Figure 1.

The transitions of Gd^{3+} in the tetragonal (C_{4v}) site of SrF_2 were examined in detail by two approaches. Both use the Ofelt-Judd[5,6] theory of induced electric-dipole transitions of RE ions in solids. One method[7] uses a direct search principle to fit the T_2 and T_6 parameters of Judd[6] to the experimental data. The other method[8] is essentially an "ab initio" approach where certain

$^6D_{7/2}$

40,707 ——— 40,587   40,574

40 —

$^6D_{9/2}$

39,681 �▅▅▅   39,556   39,562

38 —

— 11/2, 15/2, 13/2

— 9/2, 17/2

^6I

36,651 ▅▅▅   36,567   36,562
36,307 ▅▅▅   36,228   36,218
36 — 35,933 ▅▅▅D   35,850   35,832
        7/2

10^3 cm^{-1}

34 —

$^6P_{3/2}$

33,321* ——— C 33,289   33,272   33,242   33,291

$^6P_{5/2}$

32,758 ▅▅▅ B 32,717   32,700   32,671   32,716

$^6P_{7/2}$

32 — 32,167 ▅▅▅ A 32,120   32,105   32,078   32,122

SrF$_2$(Gd^{3+})^a C$_{4v}$ SITE $^8S_{7/2}$ LaCl$_3$(Gd^{3+})^b GdCl$_3\cdot$6H$_2$O^c Gd ACETATE^d Gd SULFATE^d

Figure 1. Observed Energy Centroids of Gd^{3+} in Various Hosts. [The following numbers ... the ... references cited in the REFERENCES list in the text. a, 1; b, 2; c, 3; d, 4. a - This level was observed in a 5 mole percent sample, and although it is probably not from the C$_{4v}$ site, it is indicative of the approximate position.]

assumptions concerning the character of the interactions and the crystal field are made so as to permit a direct calculation of the induced electric dipole strengths. For both cases, the experimental values of the oscillator strengths for the J-manifolds were obtained from a concentration study[1] of the C_{4v} site of Gd^{3+} in SrF_2. Papers describing these two methods and their results are in preparation. One of the important applications of line strength calculations is to the analyses of Zeeman spectra. A detailed review[8] of the theory of the Zeeman effect on RE ions (with emphasis on Gd^{3+}) in the fluorite lattice and of the required line strength calculations will be published under separate cover.

In the "direct-search" method,[7] the experimental oscillator strengths are determined by a linear least squares analysis of absorption data versus concentration. The parameters T_2 and T_6 are then fitted to the experimental strengths after the theoretical values of magnetic dipole and electric quadrupole are subtracted out. It is found that, depending on which of the states are included in the fitting routine, there are several possible sets of T_λ parameters. The set which gave the smallest χ^2 was found to be that which gives the smallest electric dipole character to the $^6P_{7/2, 5/2}$ transitions.

One noteworthy contribution in the paper describing this method, is the calculation of the line strengths using the crystal field matrix elements for the quantum mechanical basic states. The calculations showed that crystal-field J mixing is indeed small for the ^6P multiplets in the C_{4v} site but that a slight improvement is obtained between calculation and theory when J-mixing is included. Another calculation, which is rarely seen in the literature which also appears in this paper, is that of the transition strengths to individual crystal field levels within a J manifold. The Ofelt-Judd theory is usually restricted to sums of line strengths over an entire multiplet, e.g. $^6P_{7/2}$ or $^6P_{5/2}$. The agreement between experiment and calculation is excellent.

In the "ab initio" method,[8] the $T_{2, 4, 6}$ parameters are calculated directly from the theoretical expression given by Judd.[6] The nonzero values of the odd-parity crystal field coefficients are determined by calculating the point charge contributions that occur when the fluorine cell surrounding the

3

Gd^{3+} ion is distorted by the inclusion of the ninth F^- ion along the [001] direction. Two distortion parameters are defined which specify the movement of the F^- ions relative to the Gd^{3+} ion. The experimental values of oscillator strength are found by a procedure which utilizes the theoretical ratios of the strengths of the $^6P_{5/2}$ and $^6P_{7/2}$ transitions with the corresponding experimental ratios. This technique determines a set of oscillator strengths which are constrained by the current theoretical calculation and, therefore, has the advantage of giving an unique fit. The resulting values of oscillator

strength are then used to determine the values of the distortion parameters needed to fit the electric dipole content of the transitions. This method was found to be somewhat dependent on the existence of J-mixing. Free-ion values of magnetic dipole strengths do not permit a close fit to the $^6D_{9/2, 7/2}$ transitions, whereas, these strengths in the C_{4v} site including J-mixing give a more reasonable result for these ^6D_J transitions.

An additional value of this approach is that not only can the transition strengths between individual crystal-field levels be calculated but the tie between the ion placements and the induced electric dipole contributions can be determined. This is not limited to sites in which the induced electric dipole strength comes entirely from a distortion of the host symmetry. The basic concept of this method is that the induced electric dipole contribution can be related directly to the point-charge model of the surrounding ions wherein appropriate ion spacings in this complex are chosen to fit the calculated strengths to the observed values while maintaining the correct point-group symmetry and approximate angular locations of the surrounding ions as seen at the RE site.

An interesting result obtained using this last approach is that it is possible to estimate the absolute site concentrations for the three main sites, cubic (O_h), tetragonal (C_{4v}), and trigonal (C_{3v}) as functions of the Gd^{3+} concentration in a self-consistent manner. As was found in EPR studies,[9] the ratio of the cubic to axial concentrations increase with increasing Gd^{3+} concentration. As will be described in Sections 2 and 6 of this report, the same result is observed in SrF_2 doubled doped with Gd^{3+} and Ce^{3+} as a function of

4

the Ce^{3+} doping. There is, however, a significant difference between the EPR results and those obtained from the optical data. The optical data shows that in the singly doped samples, the ratio increases because the axial site concentration decreases with the cubic concentration remaining almost constant to 0.5 mole % Gd^{3+}. In the doubled doped samples,[10] the ratio increases also, but at a faster rate, primarily because of the rather sudden appearance and rapid growth of the cubic spectrum at around 0.1 mole % Ce^{3+} with the total axial concentration decreasing rapidly above 0.2 mole % Ce^{3+}. Two proposals for explaining these observations are presented in Section 2.

1.2 Er^{3+} in $YAlO_3$

The most recent work on rare earth spectra concerns the line strengths of Er^{3+} in $YAlO_3$. The polarized absorption spectra were taken by A. Santiago in the course of pursuing an Air Force Institute of Technology (AFIT) thesis. The exposures were traced by University of Dayton personnel and first analyzed to determine the extent of adverse effects such as over absorption, saturation and nonlinearities in the photographic-plate response. As a prelude to fitting the individual crystal field level transitions, the Ofelt-Judd theory was applied to the composite spectra. The results[7] are summarized in Tables I and II and in Figure 2. These data are being prepared for publication.

TABLE I

LINE STRENGTH DATA FOR Er^{3+}:$YAlO_3$

Multiplet	Energy (cm^{-1})	Expt'l	Oscillator Strength $(\times 10^{-6})$ Calc. Case I[a]	Case II[b]	Case III[c]
$^4I_{9/2}$	12,543.2	3.10	1.57	0.89	1.95
$^4F_{9/2}$	13,346.5	13.8	9.37	11.4	12.07*
$^4S_{3/2}$	18,421.6	5.61	2.29	5.04	3.11*
$^2H_{11/2}$	19,192.4	27.8	27.6	27.5	27.8 *
$^4F_{7/2}$	20,559.4	9.5	9.47	17.3	12.6 *
$^4F_{5/2}$	22,202.4	5.12	2.89	6.35	3.9
$^4F_{3/2}$	22,535.9	4.93	1.74	3.82	2.36*
$^2G_{9/2}$	24,601.8	7.50	3.66	7.47	4.93*
$^4G_{11/2}$	27,141.0	50.43	50.44	50.16	50.7
	27,433.5	22.23	25.38	39.39	32.9
$^2P_{3/2}$	31,492.1	1.40	0.34	0.74	0.46*
$^4G_{7/2}$	33,969.8	4.69	0.89	0.53	1.10
$^2D_{5/2}$	34,752.7	1.27	0.51	1.12	0.69
$^2H_{9/2}$	36,359.4	1.60	1.33	0.64	1.65
RMS Deviation $(\times 10^{-7})$			6.5	14.	6.

a) All data were fit with unit weight

b) All data were fit to obtain the three line strength parameters in sequence

c) Selected lines only were used in the fit - those with an asterisk

TABLE II

SUMMARY OF PARAMETERS FIT TO Er^{3+}:$YA\ell O_3$ LINE STRENGTH DATA

Parameter ($\times 10^{-9}$)	Case I[a]	Case II[b]	Case III[c]
T_2	13.1	13.5	12.2
T_4	5.58	2.67	6.9
T_6	4.83	10.6	6.6
RMS Deviation ($\times 10^{-7}$)	6.5	14.0	7.95
Avg Percent Deviation	39	36	34

a) All data were fit with unit weight

b) All data were fit to obtain the three line-strength parameters in sequence

c) Selected lines only were used in the fit - those with an asterisk
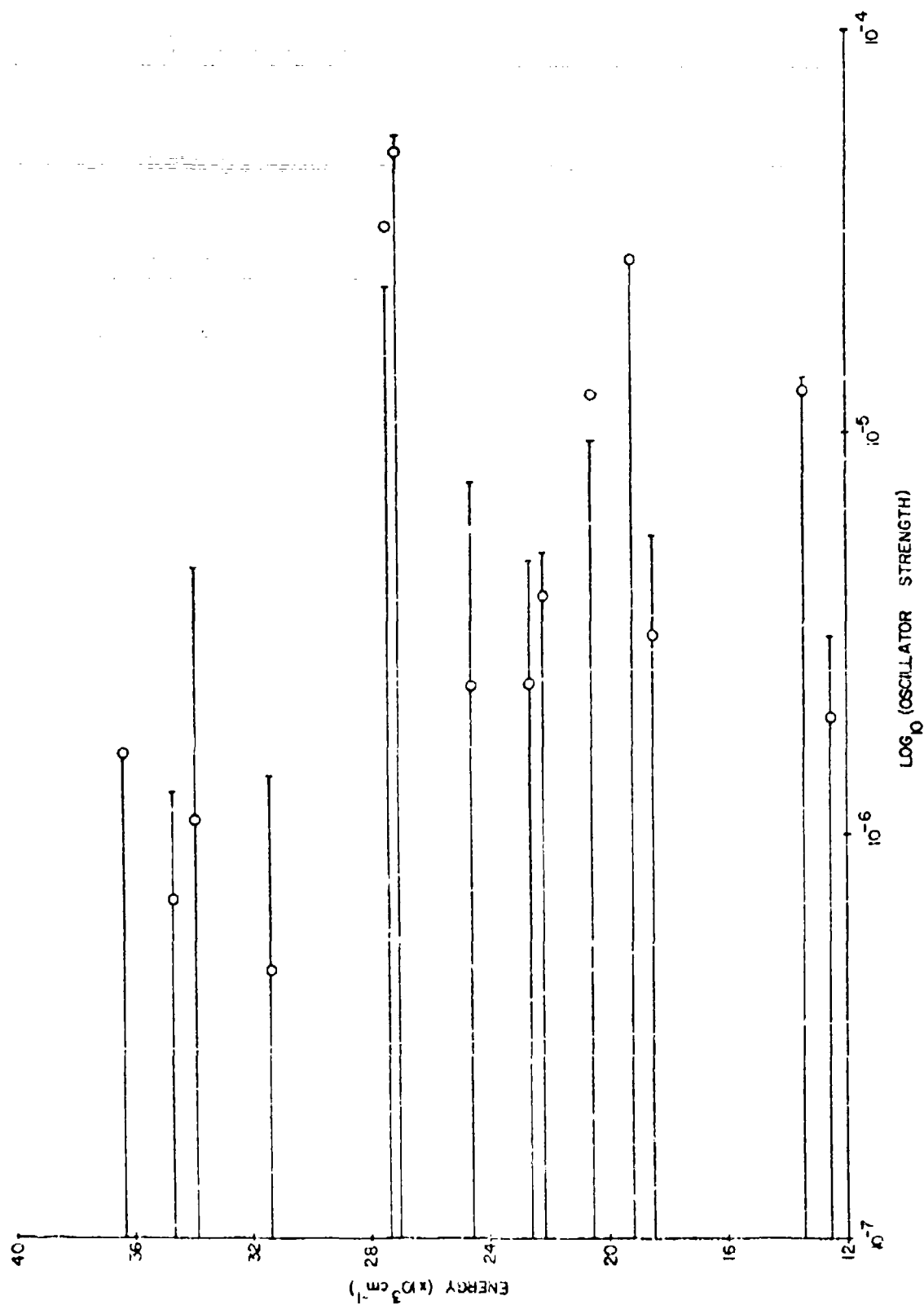
Figure 2. The Calculated (circles) and Measured (lines) Line Strengths of $Er^{3+}:YAlO_3$. [The Average Deviation is about 34% for These Data which Correspond to Case III.]

8

SECTION 2

CLUSTERING OF RE IONS IN CRYSTALS

2.1 INTRODUCTION

This area of activity arose from optical studies by Wolf and Yaney[11] and Schaeffer and Yaney[10] of SrF_2 double doped with Gd^{3+} and Ce^{3+}. These studies showed that the uv fluorescence of Gd^{3+} was enhanced by a factor of 50 to 60 by the addition of Ce^{3+}.

Continued study of the optical data and the results of EPR studies[9] revealed that the concentration of the cubic site of Gd^{3+} increased with increasing Ce^{3+} concentration in contradiction to the usual statistical mechanics predictions (see Reference 12 and the papers cited therein). Two explanations were offered to explain this behavior. The first,[13] based on the EPR results and reviewed in Section 6 of this report, purposes that the cubic site is locally compensated, that is, the Gd^{3+} ions are in large clusters, the Gd^{3+} site of which has cubic symmetry. A brief description of this model is given in the following paragraphs. The second explanation[8] assumes that the cubic site is the usual nonlocally-compensated cubic site common to RE ions in fluorites. Its behavior is then explained by assuming that Ce^{3+} acts as a "getter" for the interstitial F^- ions in the SrF_2 lattice. This model is described in some detail in Paragraph 2.3.

2.2 THE LOCAL CUBIC PHASE MODEL

It has been observed by several investigators (see Reference 12 and the papers cited therein) that as the rare earth impurity concentration is increased in fluorite crystals the relative number of cubic symmetry sites increases. This is exactly opposite to what one would expect on the basis of statistical mechanical considerations. A model has been proposed[12,13] which would resolve this discrepancy. The basic feature of the model is that a separate

phase $RF_3 : 3 (MeF_2)$ (R = rare earth ion and Me = divalent metal ion) of a
fluorite lattice exists within the crystal which preserves a cubic environment
for the tripositive rare earth ion, but for which the charge compensation
mechanism is of a local nature. The usual compensation mechanism for
cubic symmetry is of a nonlocal nature, i. e., the charge compensating
fluorine is so far away from the rare earth impurity that the point group
symmetry of the rare earth site is the cubic symmetry of the fluorite lattice.
It is the relative populations of this type of site that one would expect to de-
crease as the impurity concentration is increased.

In the local cubic phase model $R^{3+}:F^-$ defect pairs condense into a
separate phase, $RF_3 : 3 (MeF_2)$, by forming localized regions of high con-
centrations of these pairs. The point group symmetry of the rare earth
impurity sites in this phase is cubic. As the concentration of rare earth
impurities is increased more $R^{3+}:F^-$ defect pairs condense into this phase
thus explaining the increase in the relative number of cubic impurity sites.

The critical concentration at which the local cubic phase could form is
found to be

$$f = 6 \exp \left(\frac{\epsilon'}{kT} + 1 \right)$$

where f is the concentration of rare earth impurities and ϵ' is the average
excess interaction energy of attraction of a $R^{3+}:F^-$ pair in this phase with
all other pairs in the phase. By excess energy we mean the additional
energy of interaction due to the clustering of pairs. Calculations have been
carried out for the case of $SrF_2:Gd^{3+}$ and $SrF_2: (Gd^{3+}, Ce^{3+})$ which indicate
that the local cubic phase could form at concentrations as low as 0.36% total
rare earth impurity concentration.

2.3 OPTICAL STUDIES OF $SrF_2: (Gd^{3+}, Ce^{3+})$

These studies can be separated naturally into two parts; those on
absorption spectra and those on fluorescence and excitation spectra.

The fluorescence data from these samples has been reduced and the results indicate that the observed spectra is produced by three basic sites and their pair spectra. One site is the common C_{4v} site of Gd^{3+} wherein the radiation trapping phenomenon is observed in the lifetime data.[14] This is illustrated in Figure 3. This result is supported by the identification of a C_{4v} pair line in the fluorescence spectra of the samples.

The identification of additional pair lines plus other arguments based on the probability of the nearest and next-nearest neighbor clusters of Gd^{3+} and Ce^{3+} and analyses of absorption and excitation spectra have provided strong evidence for the assertion that the enhanced fluorescence output from the double-doped samples arises from Gd^{3+} and Ce^{3+} in nearest-neighbor and next-nearest-neighbor doubles clusters. These results as well as those coming from the absorption data are many fold and are being prepared for publication.

In this report we shall describe only the analysis[8] of the absorption spectra in some detail. Basically, we can show that by accounting for the association energy of Gd^{3+} - F^-_{int} pairs, the dependence of Gd^{3+} singles concentration on total RE concentration, and the probable "gettering" action of Ce^{3+} on interstitial F^- ions compared to that of Gd^{3+}, we can explain reasonably well the observed Gd^{3+} site concentration changes versus the Ce^{3+} concentration.

In brief, the fractional concentration of a fluorine compensated axial site is found from statistical mechanics arguments[12] to be approximately,

$$f_g \sim gf^2/[gf + \exp\{-\epsilon_g\}/kT]$$

where g - 6 or 8 corresponds to either the tetragonal (C_{4v}) or trigonal (C_{3v}) site, respectively, f is the fractional concentration of RE ions in single sites, and ϵ_g is the association energy of the R^{3+} - F^- pair. The singles, doubles, and triples concentrations of Me^{2+} impurity ions in simple lattices has been computed assuming next-nearest-neighbor interactions.[15] This
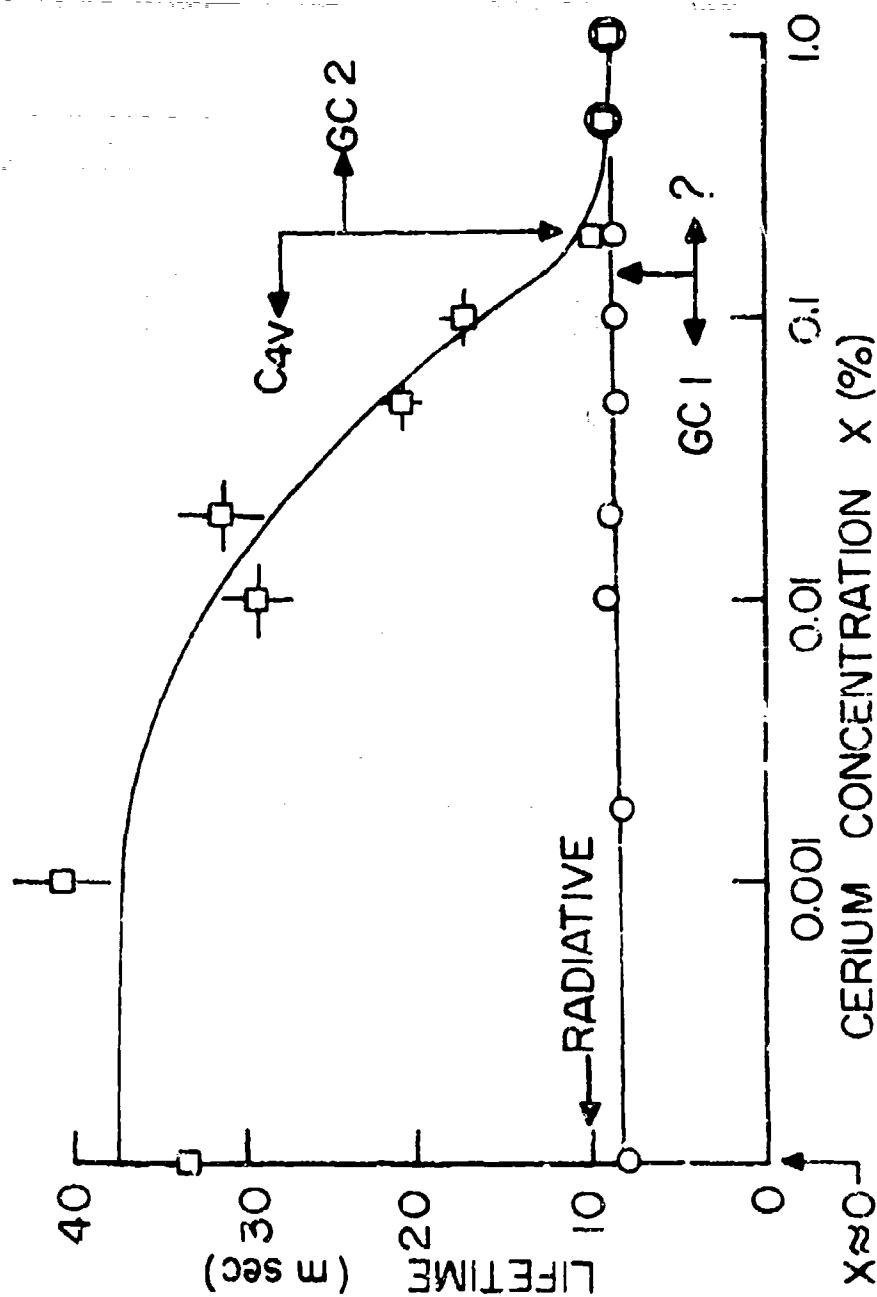
Figure 3. Observed Lifetimes of the $^6P_{7/2}$ Fluorescence of Gd^{3+} in SrF$_2$ at 77°K versus the Concentration of Codopant Ce^{3+} [The radiative value shown comes from the C_{4v} absorption spectra. Thus, radiation trapping accounts for the large C_{4v} lifetime at low Ce^{3+} concentrations. Sites GC1 and GC2 are postulated to be Gd^{3+}-Ce^{3+} nearest- and next-nearest-neighbor double clusters, respectively. See text. □ – Data taken with 2750 Å excitation. ○ – Data taken with 2500 Å excitation. The curves are hand fitted.]

12

approach can be applied to the R^{3+} ions in SrF_2 if the influence of the additional charge is neglected. For the singles concentration this analysis gives

$$f = Y (1 - Z)^{18} ,$$

where Z is the total RE fractional concentration and Y is the Gd^{3+} fractional concentration.

In order to account for the increase in the cubic concentration, we assume, consistent with ionic conductivity experiments on Nd^{3+} and Tb^{3+} in SrF_2 reported by Kristianpoller and Kirsh,[16] that the association of interstitial F^- ions with Ce^{3+} is greater than with Gd^{3+} ions. By a simple argument, we find the fractional concentration of F^- - compensated Gd^{3+} axial sites in the presence of the Ce^{3+} can be expressed by

$$f'_g = f_g [1 + G_g (X)]^{-1} ,$$

where G_g is some single-valued, monotomically increasing function of the Ce^{3+} fractional concentration X. We chose $G_g (X)$ to be

$$G_g (X) = \beta_g X^{\alpha_g} ,$$

where β_g and α_g are constants to be determined. Thus the cubic concentration is given by

$$f_c = f - \Sigma_g f'_g$$

The result of fitting this calculation to the experimental site concentrations determined from the optical absorption spectra is shown in Figure 4. The following parameters were obtained.

	C_{4v}	C_{3v}
α	1.5	1.5
β	2.4	4.0
$-|E|/kT$	-7.7₁	-3.45

where β is for X in percent.

13
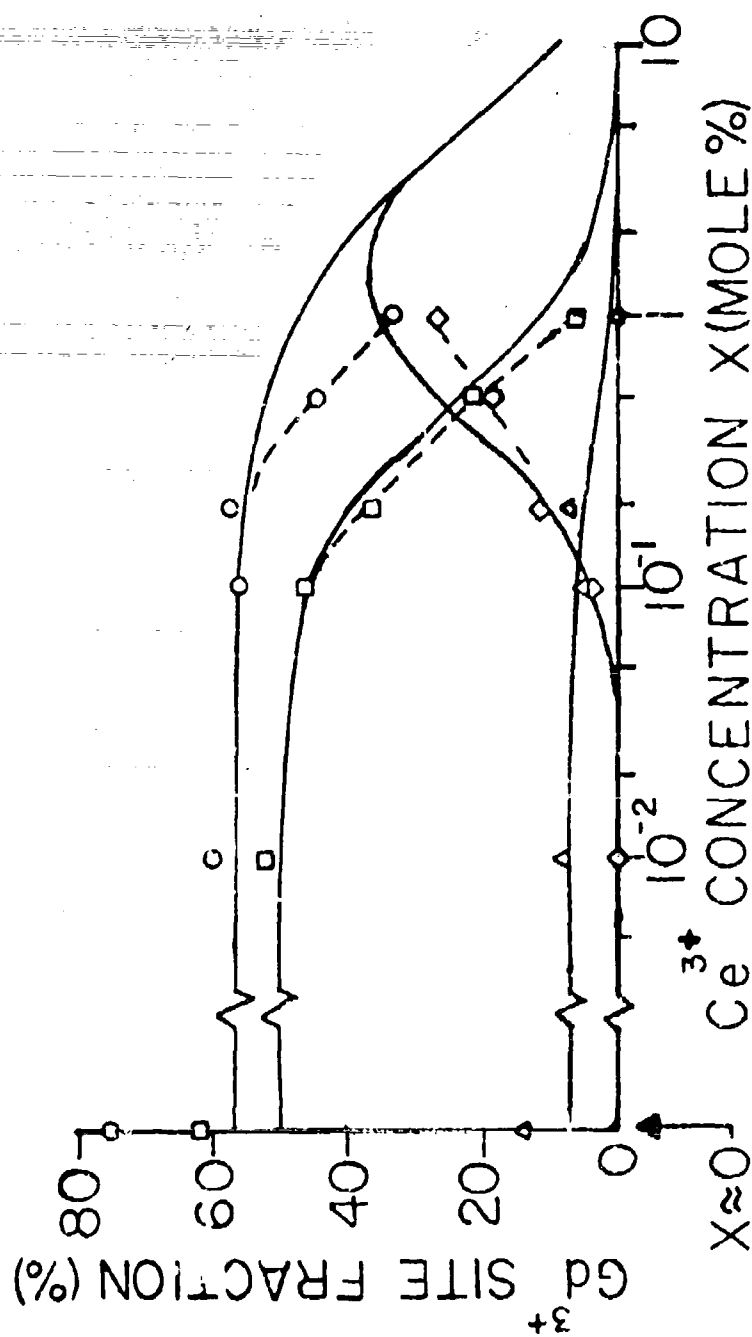
Figure 4. The Absolute Gd^{3+} site fractions in SrF$_2$ Versus the Concentration of Codopant Ce^{3+}. [The data points and dashed curves are experimental values obtained from optical absorption data: ◇ - cubic; □ - tetragonal; △ - trigonal; ○ - total of the three sites. The solid curves are calculated from the Ce^{3+} "getter" model. See text.]

14

Heist and Fong[17] have analyzed the distribution of Me^{3+}-F^- pairs in fluorite-type lattices. Using their equilibrium temperature of $630^O K$, we obtain association energies of -0.42 and -0.19 eV for the tetragonal and trigonal sites, respectively, which are to be compared to their values of -0.48 and -0.30 eV, respectively. The close agreement of the tetragonal values gives some support to the correctness of the analysis. The discrepancy between the trigonal values is really not significant in view of the uncertainties in the trigonal data. The F^- - gettering parameter value of α = 1.5 indicates that for Ce^{3+} concentrations above 2.6 mole percent, an increase in the Ce^{3+} concentration by 1/3 will reduce the tetragonal concentration by about 1/2. At a Ce^{3+} concentration of about 0.1 mole %, an increase in the Ce^{3+} concentration by 1/3 will decrease the tetragonal concentration by about 1/20. Hence, the rate of loss of axial sites with increasing Ce^{3+} concentration is greater than the rate of loss of Gd^{3+} singles concentration in the 0.1 to 1 mole % range resulting in the appearance and increasing concentration of the cubic sites.

SECTION 3

THEORETICAL AND COMPUTATIONAL STUDIES

There are three areas in which calculations have been carried out. These are line strength calculations for Er^{3+} in $YAlO_3$, free-ion and crystal field calculations, and the calculation of the term shifts due to RE-ion-ligand overlap through the B_0^0 term and the electrostatically correlated crystal field interaction.

3.1 LINE STRENGTH OF Er^{3+} in $YAlO_3$

Several tasks associated with the line strength calculations described in Section 1 of this report have been completed. The normalized tesseral harmonics of seventh order in polar and cartesian form which did not exist in the literature were worked out and these results have been published. [18]

The seventh order tesseral harmonics enter into the line strength calculations for RE spectra. In addition to developing the analytical form of these harmonics, a computer program was written to perform point-charge model lattice sums for any ion site in any arbitrary crystal structure. The present routine does not have provisions for the inclusion of a charge compensating defect or impurity, nor for including the effects of applied strain, and the local coordinate reference frame is fixed with respect to the crystallographic directions. Modifications to the program to include these considerations are planned for implementation as the need arises.

An example of the calculation for the Y-site in $YAlO_3$ is given in Table III. This site possesses C_s symmetry with the mirror plane perpendicular to the crystallographic c-axis. The calculation is in substantial quantitative agreement with preliminary calculations of the spectra

TABLE III

LATTICE SUMS FOR ALL[a] TERMS IN THE CRYSTAL FIELD
EXPANSION FOR THE Y-SITE (C_s) IN $YA\ell O_3$[b]

Coefficient	B_q^k Coefficient (cm^{-1})	
	Real	Imaginary
B_1^1	-1110.1	-329.8
B_0^2	- 509.7	0
B_2^2	4754.1	-211.0
B_1^3	193.3	46.1
B_3^3	323.2	-738.8
B_0^4	- 202.9	0
B_2^4	- 144.9	- 45.0
B_4^4	- 96.0	57.6
B_1^5	38.2	- 28.5
B_3^5	92.1	- 72.8
B_5^5	- 20.4	- 92.1
B_0^6	- 10.1	0
B_2^6	9.44	- 5.74
B_4^6	- 35.6	13.0
B_6^6	9.64	- 4.5
B_1^7	1.52	- 0.31
B_3^7	- 1.79	- 0.42
B_5^7	2.48	- 2.32
B_7^7	- 1.77	1.71

a) All terms for which k + q is Odd are zero

b) These signs are appropriate for the site at the location (0.018, -0.06, -0.25)

based on fitting the observed energy levels. (See Paragraph 3.3). The qualitative agreement with group theoretical expectations with respect to the nonzero elements is, of course, exact. Although point-charge model calculations leave much to be desired in predicting RE spectra, this work is justified by the need to properly orient the quantum mechanical basis vectors with respect to the crystallographic axes to insure the proper interpretation of polarized absorption spectra. It is important that the site coordinates agree with the coordinates implied by the angular momentum projections (J_z) whose linear combination defines a given crystal field level and its orientation in space. The signs of the various lattice sums determine these phase considerations and can be used to insure that the basis states are aligned with the experimentally defined directions. This program is still being developed and no listing is included in this report.

3.2 FREE ION ENERGY LEVEL CALCULATIONS

Calculations of the free ion spectra of rare earth ions have been extended to include the effect of three body operators.[19-21] The Hamiltonian for a free ion with an f^N configuration can be accurately represented by effective operators which include Coulomb, spin-orbit, configuration, spin-spin, and spin-other-orbit interactions. The configuration interactions which account for Coulomb interaction between f^N and configurations which differ from f^N by the excitation of two electrons are included through second order perturbation theory via two body operators. These two body operators introduce the adjustable parameters α, β, and γ into the effective Hamiltonian.

The perturbing effects of the Coulomb interaction between f^N and configurations which differ from f^N by single particle excitations, i. e., $(n\ell)^{N-1}(n'\ell')$ or $(n\ell)^{N+1}(n'\ell')^{4\ell'+1}$, can be included through second order perturbation theory by the introduction of effective two body and three body operators. The two body parts are absorbed by the parameters of two body operators already present in the effective Hamiltonian.

18

Judd[21] has shown that the effects of the three body operators can be included by the addition of six terms, $t_i T^i$ (i = 2, 3, 4, 6, 7, 8), to the effective Hamiltonian. The quantities t_i are effective three body operators and T^i are adjustable parameters.

We have determined the matrix elements of the three body operators for all of the configurations f^3 to f^{11}. These matrix elements now exist in a form such that the Hamiltonian

$$H = E^1 \epsilon_1 + E^2 \epsilon_2 + E^3 \epsilon_3 + \xi \sum_i \vec{s}_i \cdot \vec{\ell}_i + \alpha L(L+1) + \beta G(G_2) + \gamma G(R_7)$$

$$+ H_{ss}(M^0, M^2, M^4) + H_{soo}(M^0, M^2, M^4) + H_{ci}(P^2, P^4, P^6) + \sum_{\substack{i=2,8 \\ i \neq 5}} t_i T^i$$

can be readily diagonalized for any configuration of f^N and the adjustable parameters E^1, E^2, E^3, ξ, α, β, γ, M^0, M^2, M^4, P^2, P^4, P^6, T^2, T^3, T^4, T^6, T^7, and T^8 fit to the experimental data by computer programs. The terms H_{ss}, H_{soo}, and H_{ci} stand for spin-spin, spin-other-orbit, and electrostatically correlated spin orbit interactions, respectively.[22, 23] With the inclusion of the three body operators we are thus able to determine the free ion energy levels and state vectors using all of the interactions which are to date deemed significant.

At present we have carried out these calculations on two systems, $YA\ell G:Nd^{3+}$ and $YA\ell O_3:Er^{3+}$. When the three body operators were included, the RMS error between experimental and calculated free ion centers of gravity was reduced significantly. The state vectors from these free ion calculations are now being used in crystal field calculations which will allow for the identification of more experimental energy levels. The identification of more experimental levels in turn allows for improvement in the calculations. This process will continue until there is maximum agreement between observed and calculated energy levels.

3.3 CRYSTAL FIELD CALCULATIONS

Crystal field calculations have been completed for the C_{4v} symmetry site of $SrF_2:Gd^{3+}$ and the results are published in the literature.[24] These calculations determined the crystal field coefficients, $B_q^{(k)}$'s, necessary to obtain agreement between calculated and experimental energy levels. In addition the calculation illustrates the importance of including J-mixing in crystal field calculations.

Crystal field calculations have been initiated and are continuing in order to determine the energy levels of $YA\ell O_3:Er^{3+}$. The symmetry site of the Er^{3+} ion in $YA\ell O_3$ has the point group symmetry C_s. Thus, the perturbation term in the Hamiltonian due to the crystal field interaction is,

$$
\begin{aligned}
H_{CF} = \sum_i [\; & B_0^2(C_0^2)_i + B_2^2(C_2^2 + C_{-2}^2) + i\,B'^2_2(C_2^2 - C_{-2}^2)_i + B_0^4(C_0^4)_i \\
+ \; & B_2^4(C_2^4 + C_{-2}^4)_i + iB'^4_2(C_2^4 - C_{-2}^4)_i + B_4^4(C_4^4 + C_{-4}^4)_i + iB'^4_4(C_4^4 - C_{-4}^4)_i \\
+ \; & B_0^6(C_0^6)_i + B_2^6(C_2^6 + C_{-2}^6)_i + iB'^6_2(C_2^6 - C_{-2}^6)_i + B_4^6(C_4^6 + C_4^6) \\
+ \; & iB'^6_4(C_4^6 - C_{-4}^6)_i + B_6^6(C_6^6 + C_{-6}^6)_i + iB'^6_6(C_6^6 - C_{-6}^6)_i].
\end{aligned}
$$

This shows that a complete specification of the crystal field of $YA\ell O_3:Er^{3+}$ will require the minimization of fifteen parameters which are real and imaginary. We are currently modifying the computer programs which fit the crystal parameters to the observed spectra so that the complex coefficients can be included in the diagona 'zation and fitting routines. In the past it has been the practice to assume that the complex coefficients are small and thus drop those terms from the Hamiltonian. Preliminary calculations, however, indicate that the imaginary terms are not insignificant and should be included in the fit.

3.4 CALCULATION OF TERM SHIFTS

A problem of long standing in crystal field calculations is the problem of center-of-gravity shifts due to the host lattice. The three fluorite hosts MeF_2 (Me = Ca, Sr, Ba) provide an ideal set of crystal fields of identical symmetry but different strengths to observe these shifts.[28]

A composite of the optical absorption spectra for the $^6P_{7/2}$ and $^6P_{5/2}$ states of Gd^{3+} in these hosts is given in Figure 5. Table IV presents a summary of the position measurements on these spectra. These data are averages taken over several independent high resolution studies. It is interesting to note that we found[8] that the BaF_2 lines shifted on the order of $1cm^{-1}$ in an anomalous manner with increasing Gd^{3+} concentration in the range shown in Figure 5. The other two hosts did not present a similar behavior, the line positions being essentially independent of Gd^{3+} concentration as generally would be expected. The analysis of the BaF_2 data is not complete, and therefore, will not be discussed further. However, it is interesting to point out that the Gd^{3+}-ligand overlap required to describe the term shifts could also be at the root of the BaF_2 anomally.

The outstanding feature of the spectra in Figure 5 is that regardless of the site, all the lines shift to high energies as the lattice becomes larger (i. e. Ca to Ba). This effect is most evident in Table IV in the $\Delta v_{c.g.}$ entries. Clearly, there is little deviation in these values with site symmetry or between the two states. A more dramatic presentation of these data is given in the composite energy level diagram in Figure 6. The plotting of the approximate "free-ion" positions of the states shows another interesting fact, namely that the site spectra do not approach these positions as the lattice enlarges, but rather they cross them. This fact indicates that the term position determined from the approximate "free-ion" calculation[22, 28] based on Gd^{3+} in the $LaCl_3$ host[2] is also

21
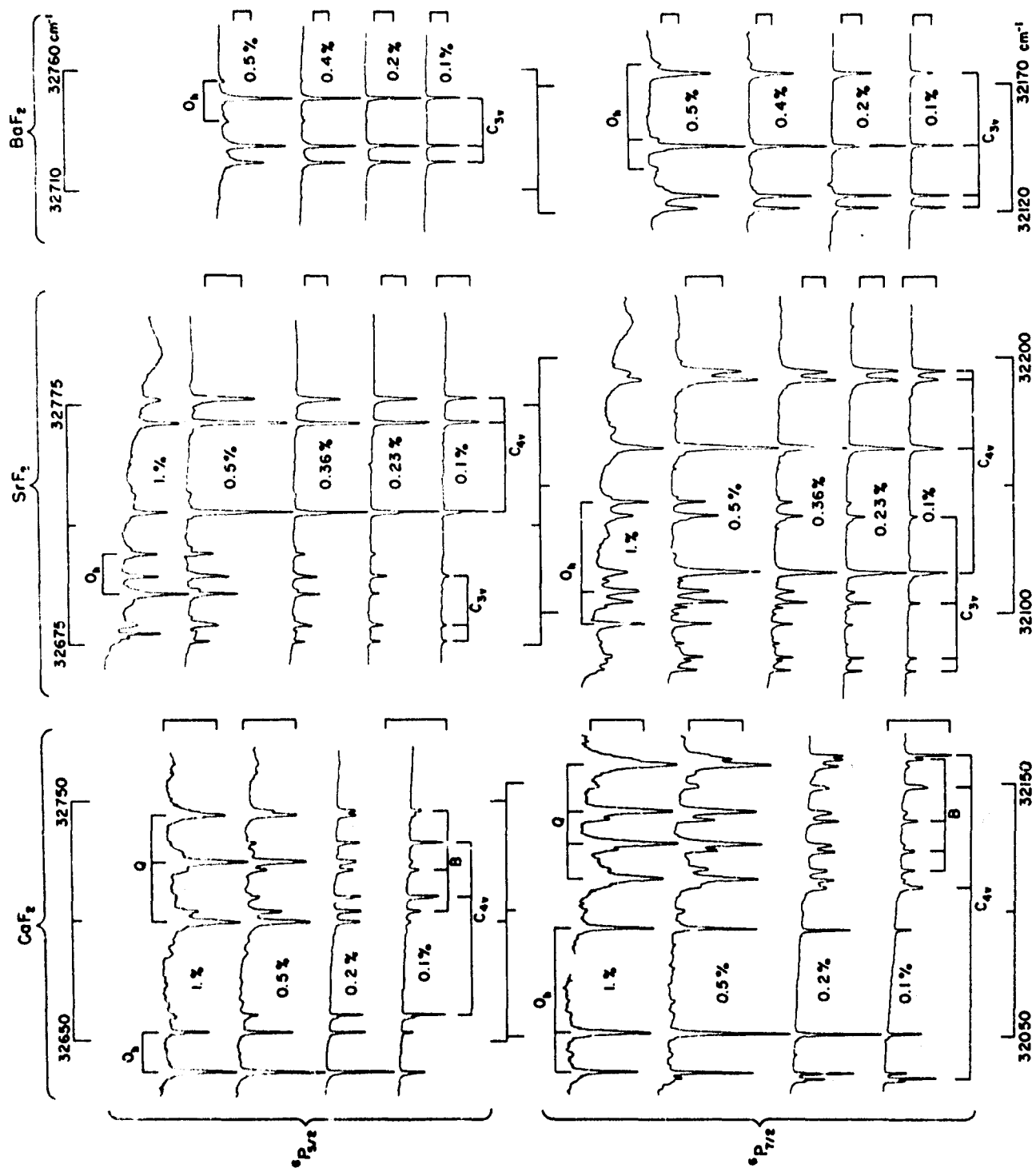
Figure 5. A Composite of the $77^\circ K$ Absorption Spectra of the $^6P_{7/2}$ and $^6P_{5/2}$ states of Gd^{3+} in Ca, Sr, and BaF_2 Over a Range of Gd^{3+} Concentrations. [The identities of the lines are after Makovsky and Gilfanov, et. al, text reference numbers 25 and 26, respectively.]

TABLE IV

VACUUM WAVENUMBER POSITIONS AND CRYSTAL FIELD SPLITTINGS OF THE $^6P_{7/2}$ and $^6P_{5/2}$ STATES OF Gd^{3+} IN THE **DOMINANT** SITES OF Ca, Sr, and BaF_2 at 77°K. [All values in cm^{-1} a - These values are in substantial agreement with those reported by Makovsky and by Gilfanov, et. a., text reference numbers 25 and 26, respectively. b- Site identification per Makovsky (ibid.) c - The C_{3v} site in CaF_2 has been reported only by Makovsky (ibid.) and only in fluorescence from the $^6P_{7/2}$ state.]

ν_{vac} (Sr) [a]	SITE [b]	$\nu_{c.g.}$ (Sr)	$\Delta\nu_{c.g.}$ Ba - Sr	$\Delta\nu_{c.g.}$ Sr - Ca	$\Delta\nu$ (from $\nu_{c.g.}$) Ba	Sr	Ca	$\Delta\nu$ (overall) Ba	Sr	Ca
$^6P_{7/2}$										
32,095.4	O_h	32,113.7	39.7	56.2	-16.4	-18.3	-21.9	41.8	47.9	56.8
32,108.1					- 4.5	- 5.6	- 6.6			
32,143.3					+25.4	+29.6	+34.9			
32,077.3	C_{3v} [c]	32,100.3	42.0	57.8	-20.7	-23.0	-25.4	53.5	60.4	67.6
32,082.4					17.5	-17.9	-19.2			
32,103.9					+ 3.7	+ 3.6	+ 2.5			
32,137.7					+32.8	+37.4	+42.2			
32,115.8	C_{4v}	32,166.9	—	53.9	---	-51.1	-79.3	—	79.3	127.4
32,164.8						- 2.1	- 4.0			
32,191.8						+24.9	+35.8			
32,195.1						+28.2	+47.8			
Ca { 32,112.4	Q	32,133.6 (Ca)	—	—	—	—	-21.2	—	—	44.7
32,126.1							- 7.5			
32,138.9							+ 5.3			
32,157.1							+23.5			
Ca { 32,115.7	B	32,133.4 (Ca)	—	—	—	—	-17.7	—	—	43.6
32,123.4							-10.0			
32,135.0							+ 1.6			
32,159.3							+25.9			
$^6P_{5/2}$										
32,696.3	O_h	32,701.9	42.7	59.1	- 5.5	- 5.6	- 5.5	16.4	16.8	16.4
32,713.1					+10.9	+11.2	+10.9			
32,676.7	C_{3v}	32,688.1	44.5	—	-11.2	-11.4	—	26.7	27.4	—
32,683.6					- 4.4	- 4.5				
32,704.1					+15.5	+16.0				
32,730.3	C_{4v}	32,758.4	—	57.5	—	-28.1	-40.3	—	47.2	72.1
32,767.5						+ 9.1	+ 8.6			
32,777.5						+19.1	+31.8			
Ca { 32,699.8	Q	32,723.0 (Ca)	—	—	—	—	-23.2	—	—	44.5
32,724.9							+ 1.9			
32,744.3							+21.3			
Ca { 32,703.8	B	32,723.4 (Ca)	—	—	—	—	-19.6	—	—	41.9
32,720.8							- 26			
32,745.7							+22.3			

Figure 6. Composite Energy Level Diagram of the $^6P_{7/2}$ and $^6P_{5/2}$ States of Gd^{3+} in the Dominant Sites of Ca, Sr, and BaF$_2$. [The solid lines are for 77°K and the two-segment broken lines are for 300°K. a - The two dashed lines extending across the diagram are the approximate "free-ion" positions calculated by O'Hare and Donlan, text reference number 27, using the parameters of Judd et. al., text reference number 22. b - The identification of the cubic crystal field levels is after O-Hare and Donlan (ibid.). c - The C_{3v} site in CaF$_2$ has been reported only by Makovsky, text reference number 25, and only in fluorescence d - Site identification per Makovsky (ibid.).]

24

shifted from the true free-ion position, as would be expected. Furthermore, the fact that the shift is essentially independent of the J value suggests that the shift depends primarily on the SL character of the state.

In order to reveal the SL dependent part of the observed shifts it was necessary to estimate the positions of the $^6P_{3/2}$ state. By applying the Landé interval rule to the $^6P_{7/2, 5/2, 3/2}$ states observed in other hosts[2-4] (see Figure 1), we were able to estimate the positions of the unobservable $^6P_{3/2}$ state in the various sites of the three fluorite hosts. This allowed the calculations of the positions of the ^6P term for the experimental case.

In order to emphasize the differences between the calculated shifts and splittings and those observed, the approximate "free-ion" values were subtracted from the data. The results of this data reduction are summarized in Figures 7 and 8. The former shows the deviation of the calculated spin-orbit splitting from the observed values for the cubic site. The $^6P_{3/2}$ experimental data are not shown because their deviations are on the same order of magnitude as the uncertainty in their positions. We shall not be concerned further at this writing with these data.

We are principally concerned with the data given in Figure 8. The straight line fits to the points are given only to show the general trend of the data. The calculated shifts are the result of J mixing. Thus, concentrating now on the cubic data, we see that subtracting the calculated shifts from the observed shifts provides the data to which we must fit our calculation.

Rajnak and Wybourne[29] have described how term shifts can occur differently for different SL states through configuration interaction in a second order perturbation calculation in which the electron-electron electrostatic interaction couples to the crystal field interaction via the B_0^0 term. However, in order to obtain a nonzero value[30] the overlap between the RE ion and the surrounding ligands must be estimated. Only the 5f configuration is involved and we find the following values for the
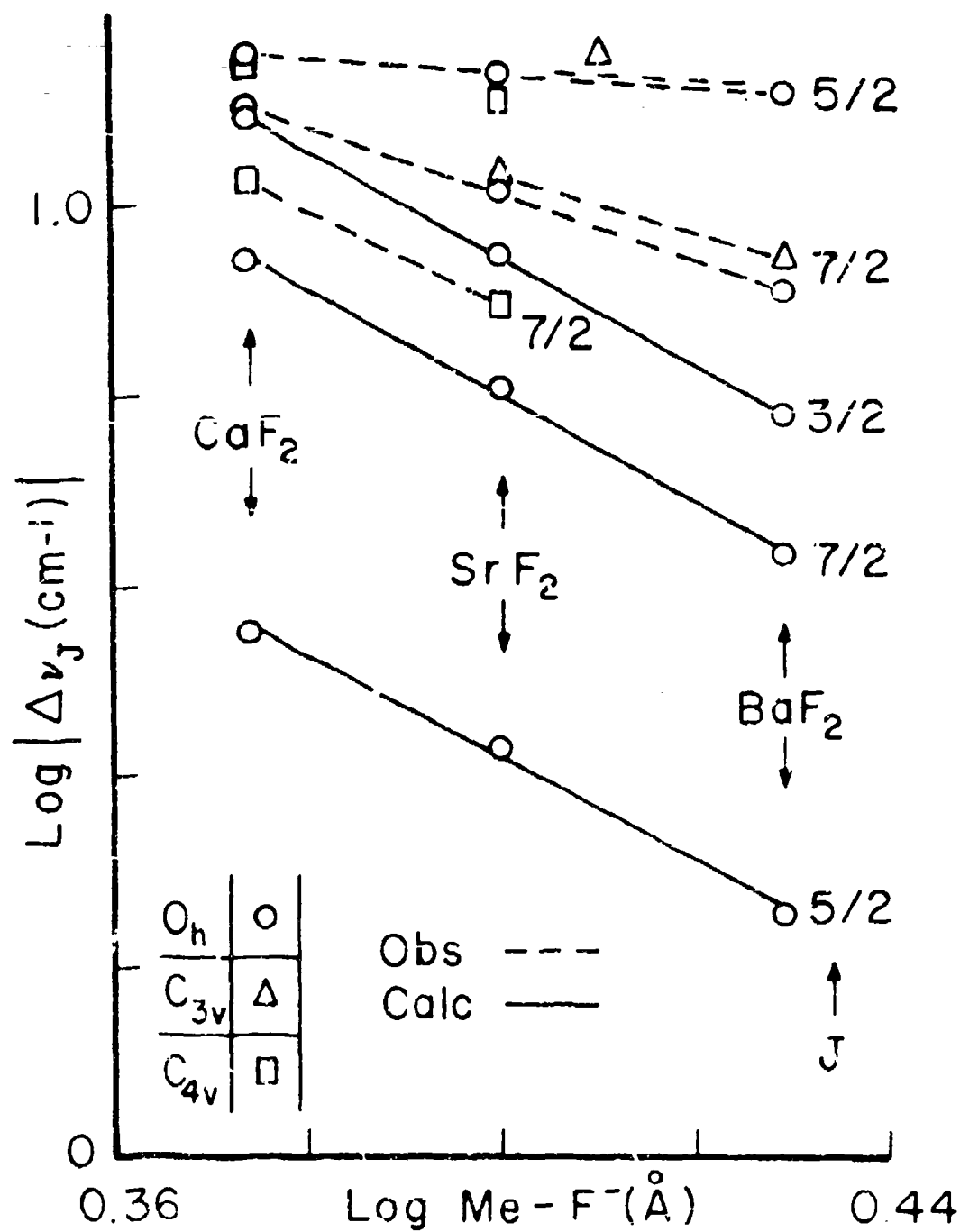
Figure 7. The Deviations of the Observed (77°K) and Calculated Spin-Orbit Splittings from the Approximate "free-ion" Values of the ^6P_J States of Gd^{3+} for the Ca, Sr, and BaF_2 hosts. [$\Delta\nu_J = | \nu_{Jcg}$ (site) $- \nu_{cg}$ (site)| $- | \nu_{Jcg}$ ("free-ion") $- \nu_{cg}$ ("free-ion")|, where J = 7/2, 5/2, and 3/2. The "free-ion" and cubic calculations are after O'Hare and Donlan, text reference number 27. See text and Figure 6.]

26.
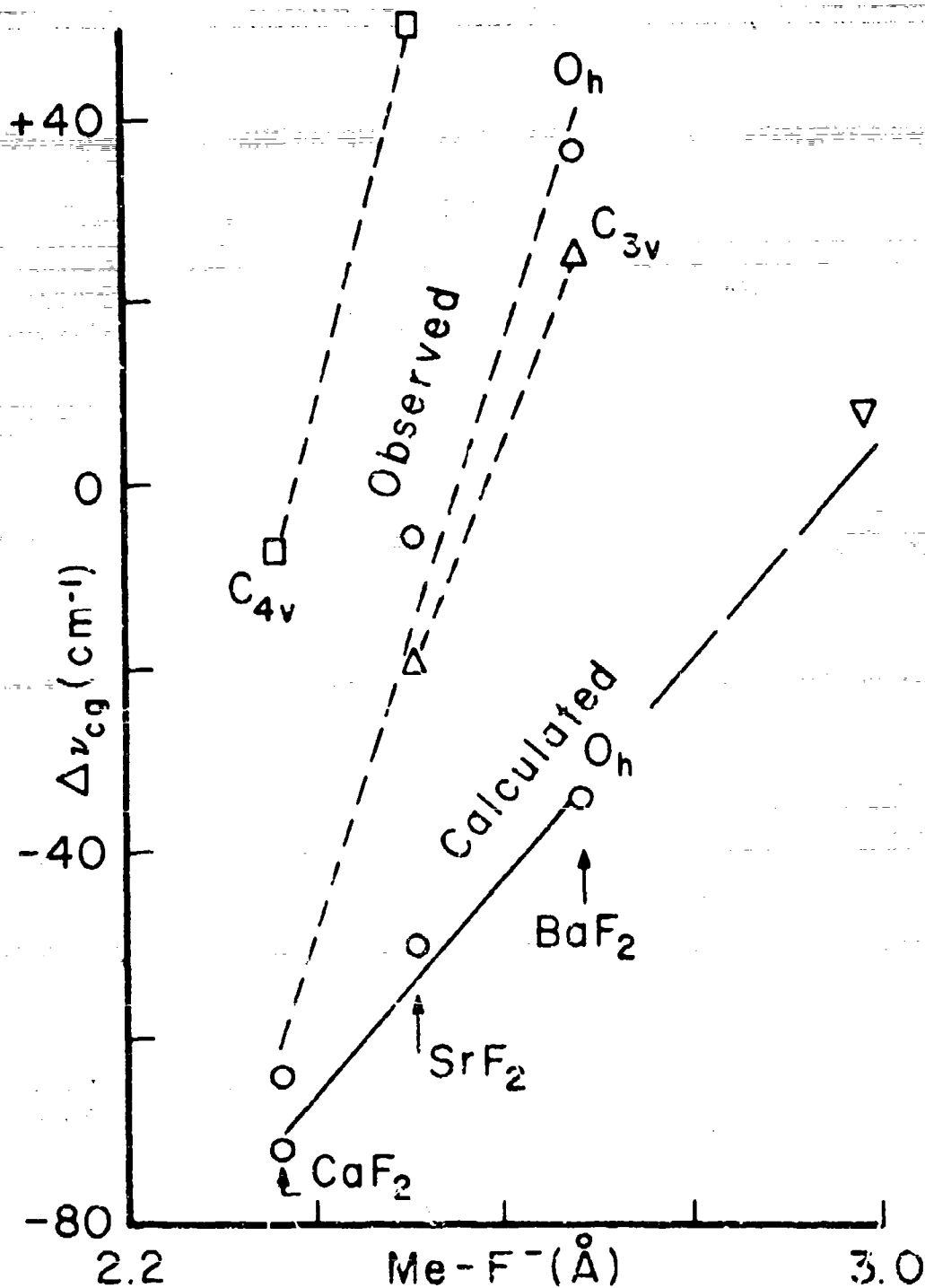
Figure 8. The Shifts of the Observed (77°K) and Calculated ^6P term Positions from the Approximate "free-ion" Values of Gd^{3+} versus the $Me^{2+}-F^-$ Spacing in the MeF_2 (Me = Ca, Sr, Ba) Hosts. [$\Delta\nu_{cg} = \nu_{cg}$ (site $^6P_{cg}$) - ν_{cg} ("free-ion" $^6P_{cg}$). See text and Figures 6 and 7. The point $\triangledown$ gives the approximate location of the ^6P term position in the "free-ion" host $LaCl_3$ after Piksis et. al., text reference number 2.]

27

$<[4f] | [5f]>$ integral where the brackets denote the expansion of the RE wave functions to include the ligand wave functions. The $Me^{2+}-F^-$ distance R_{+-} used in these calculations are also given.

Host	$<[4f]	[5f]>$	$R_{+-} (Å)$
CaF_2	-2.73×10^{-2}	2.365
SrF_2	-1.97	2.511
BaF_2	-1.32	2.685

Using these overlap integrals with the calculation described by Rajnak and Wybourne we arrive at the following theoretical term shifts.

	CaF_2	SrF_2	BaF_2
$^8S - ^6P$	-222.6	-151.5	-94.9 cm
^6I	-221.3	-150.6	-94.3
^6D	-259.8	-176.8	-110.7

It can be shown that the following expression relates the experimental to the calculated centers-of-gravity.

$$\Delta \nu_{cg}(\exp) = \Delta \nu_{cg}(\text{calc}) + \nu_r + \Delta E_0^0,$$

where ΔE_0^0 is the value given in the above table and ν_r is the reference energy which is approximately given by,

$$\nu_r \cong -\Delta E_0^0 \text{ ("free-ion" host)},$$

and the $\Delta \nu$'s are the values measured relative to the approximate free-ion values. A least squares analysis of the $\Delta \nu_{cg}(\exp) - \Delta \nu_{cg}(\text{calc})$ versus ΔE_0^0 function for the $^8S - ^6I$ energy separation gives an excellent fit

to a straight line with slope of 0.49 ± 0.02 and intercept of $118 \pm 3 \text{ cm}^{-1}$. The uncertainties are due to the deviations of the ordinate values from the fitted line. Thus, the $LaCl_3$ "free-ion" host has a $\Delta E_0^0 \simeq 118 \text{ cm}^{-1}$ shift from the true "free-ion" position for the $^8S - ^6P$ energy separation. That the slope is not unity as predicted is of little importance since there were many factors used in this calculation which were, at best, approximate. The quantity ΔE_0^0 has a fairly well-defined functional dependence on the R_{+-} distance. This is given by the following expression.

$$\Delta E_0^0 = -\frac{A}{R_{+-}} \left(B - \frac{C}{R_{+-}} \right),$$

where A, B, and C all > 0.

The parameter A includes the Madelung constant at the cation site and depends on the SL character of the two states. The parameters B and C are determined by the details of the RE ligand overlap. Basically, the calculation described here determines the ratios of the values of A that belong to different pairs of states and the ratio C/B. Specific values for the product AB and for the reference energy ν_r can then be determined by fitting them to the experimental data. A paper describing the details of this calculation is in preparation.[8]

SECTION 4

EXPERIMENTAL LASER MATERIALS STUDIES

Considerable effort has been devoted to constructing an experimental facility at the Air Force Materials Laboratory (AFML) for the evaluation of laser materials. This work has progressed along the following logical outline. Initial measurements and preliminary experiments, to be described below, were performed on a Nd:FAP Nd: $Ca_5 (PO_4)_3 F$ and a Nd:$YAlO_3$ laser rod. Following these early tests a more elaborate experimental program was outlined and the equipment necessary for its implementation was either constructed in the University of Dayton Research Institute (UDRI) shops or provided by AFML.

This experimental capability has a two-fold purpose: laser materials testing and nonlinear optical materials evaluation (SHG). These two tasks are related in that a high quality laser system is required for successful SHG materials studies. However, the laser materials evaluation must be designed to include such a wide variety of capabilities that several different facilities are actually required. The progress towards the accomplishments of these goals will be described in the following paragraphs: 1) Initial experiments and results, and 2) materials evaluation experiments under construction. It must be pointed out that no experimental capability of this type existed within the laboratory at the start of this contract and only a limited capital budget was available. Hence, this facility is still in its early stages of development.

The Nd:FAP laser rod initially presented for evaluation was 0.390-inch in diameter and 6-inches long. This was the largest rod to be studied since in most cases the laser materials suppliers under contract to AFML are to provide rods of 3 mm to 1/4-inch diameter and from 30 mm to 3-inches long. This wide range of rod diameter provided a considerable challenge in the design of a laser pump cavity or "laser head". The proper design of a pump cavity requires that the designer start with a

laser rod, preferably with known pumping characteristics and efficiency. With this information the designer selects an appropriate pump source (in this case, a flashlamp since pulsed operation is desired) and cavity configuration. Because of the large rod diameter and correspondingly large flashlamp size the minimum size ellipse of optimum aspect ratio for maximum pump efficiency was over six inches long with a minor axis of 3-inches and a major axis 5-inches long. It was also desirable to vary the relative positions of the flashtube and laser rod within the ellipse in order to obtain engineering data for future designs. There was also a requirement for the cooling of the laser rod including liquid N_2 cooling and the need for spectral filtering of the pump radiation to prevent solarization by the ultraviolet emission from the lamps. Figures 9 through 11 are drawings of the apparatus constructed to achieve these design goals. Suitable detectors for monitoring the power output had to be constructed. A cone calorimeter using a differential heating principle is used to measure total power output. A typical output pulse from the cone calorimeter is shown in Figure 12. An RCA 922 vacuum photodiode detector provided a fast response detector at 1.06 μm at a nominal cost.

The FAP rod was installed, in the pump cavity previously described, with a resonant cavity consisting of a 99.5% total reflector and only the fresnel reflection from the front of the rod as the output coupler.

Alignment was accomplished initially with the aid of a HeNe laser and finally optimized by alternately adjusting the mirrors and firing the laser at a fixed pump energy until the maximum output energy was indicated by means of an uncalibrated ballistic calorimeter.

With the laser rod at or near one focal point of the ellipse the flashlamp was moved along the major axis of the ellipse until a maximum output energy was obtained with a fixed lamp input (see Figure 13).

31
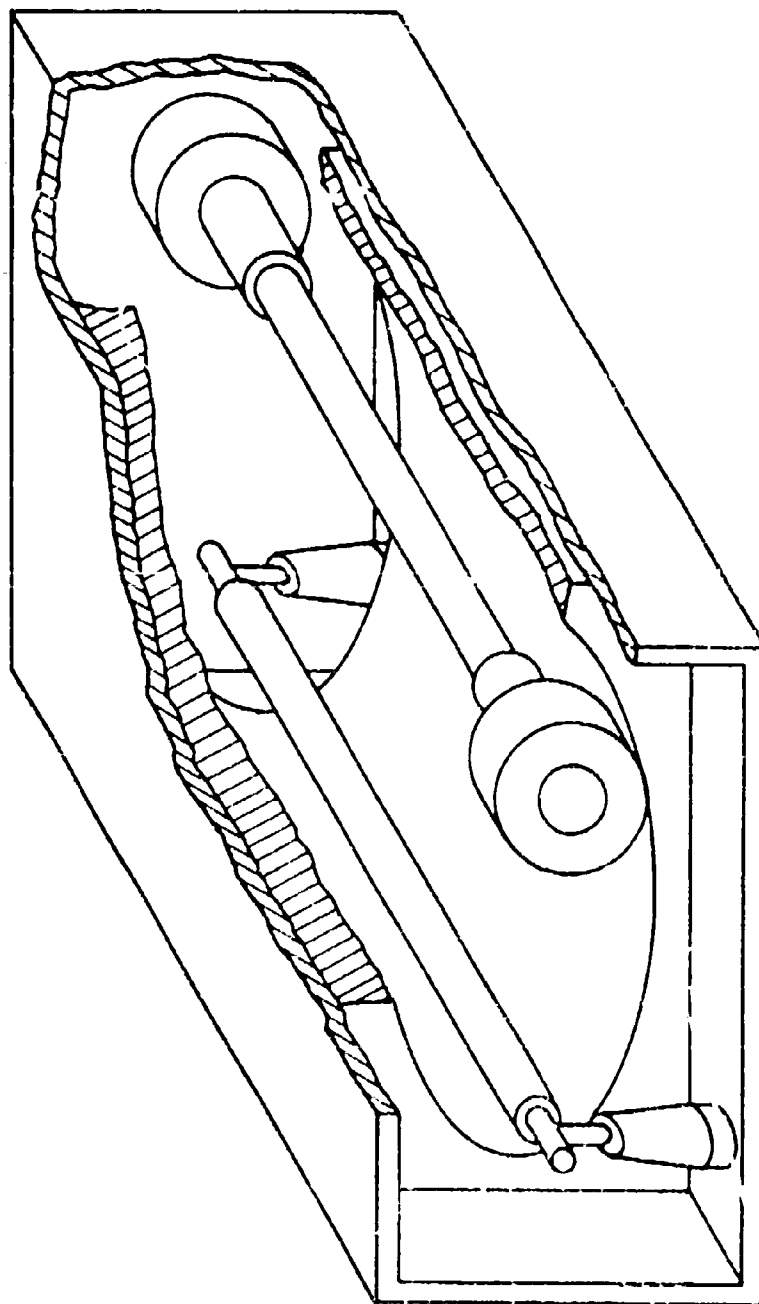
Figure 9. Cutaway View of the Single Elliptical Cavity Fabricated for Pumping the Nd^{3+}:FAP Laser Rod. (The Flashlamp is Located on the Left At One Focus of the Ellipse.)
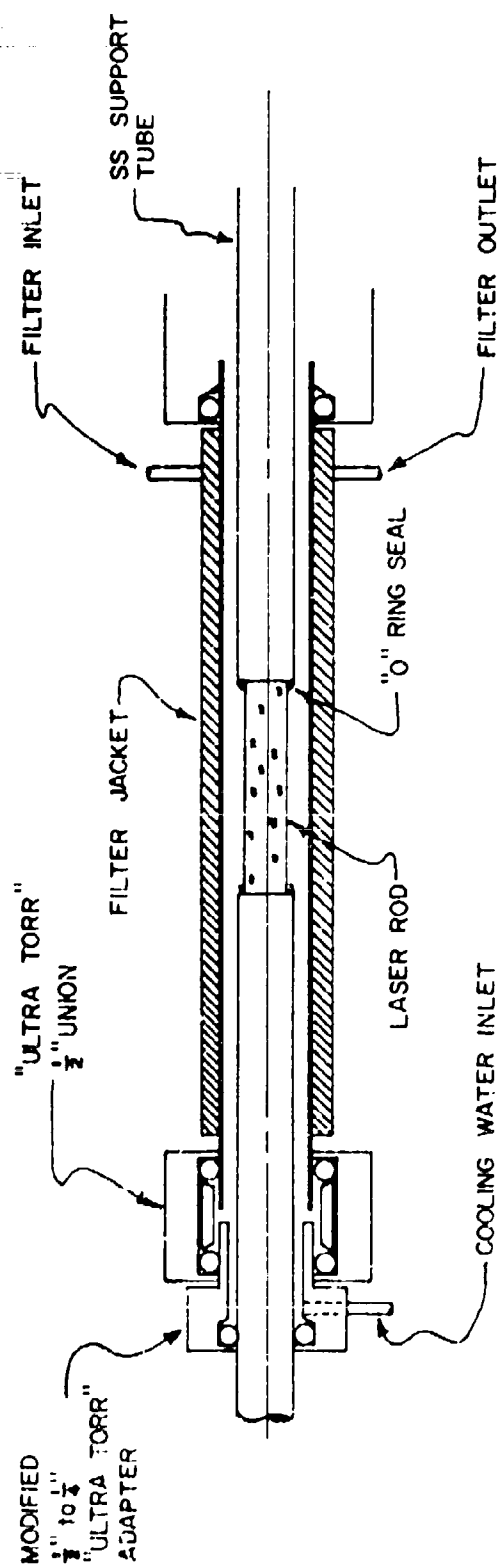
Figure 10. The Water Cooled Laser Rod Holder and Liquid Filter Assembly Fabricated at University of Dayton Research Institute to Hold a Variety of Laser Rods.

SS SUPPORT TUBE

FILTER INLET

FILTER OUTLET

"O" RING SEAL

FILTER JACKET

LASER ROD

"ULTRA TORR" ½" UNION

COOLING WATER INLET

MODIFIED ½" to ¼" "ULTRA TORR" ADAPTER

33
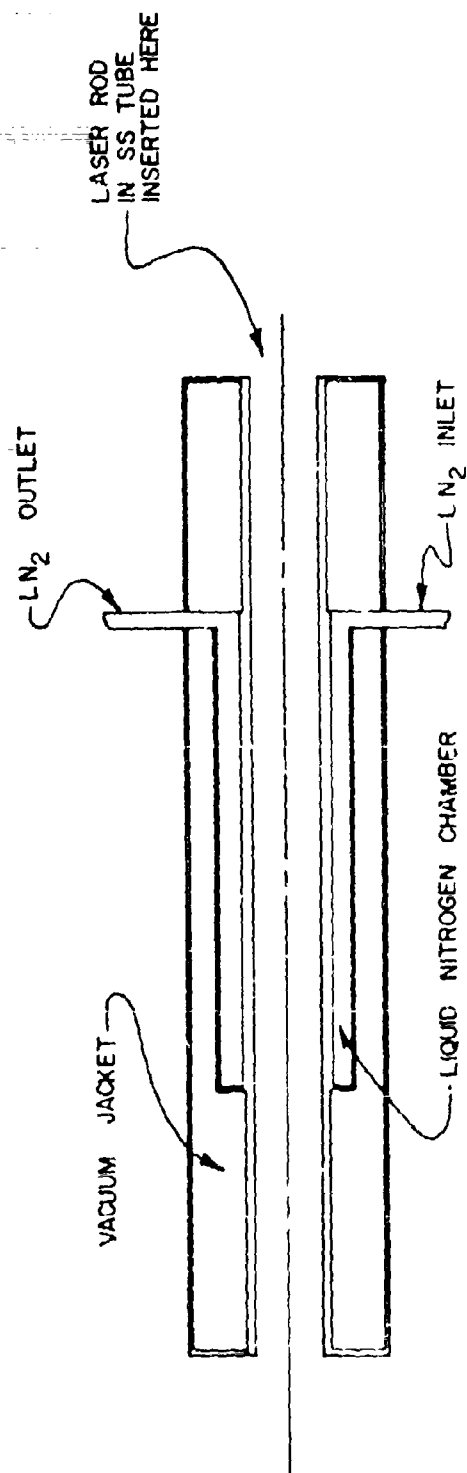
Figure 11. The Liquid Nitrogen Dewar Mount for Holding Laser Rods at Near Liquid Nitrogen Temperatures. [This Dewar can be Inserted into the Elliptical Cavity in Place of the Water Cooled Rod Holder.]

34
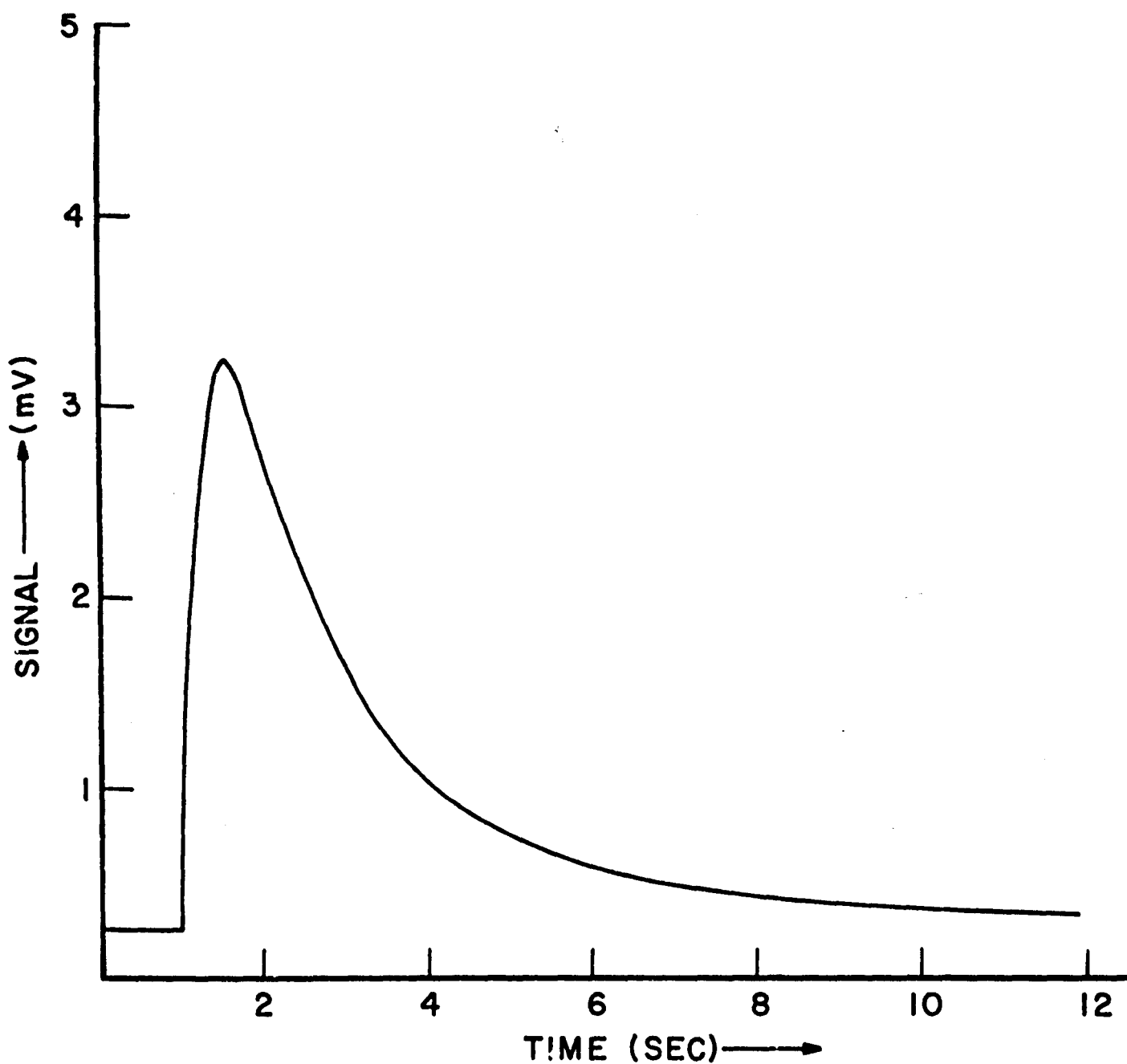
Figure 17. A Sample Trace of the Signal Obtained from the Cone
Calorimeter Fabricated by University of Dayton Research Institute
Personnel for Measuring Pulsed Laser Output Energy. [This Device
has About Twice the Sensitivity of a Similar Commercial Device.]
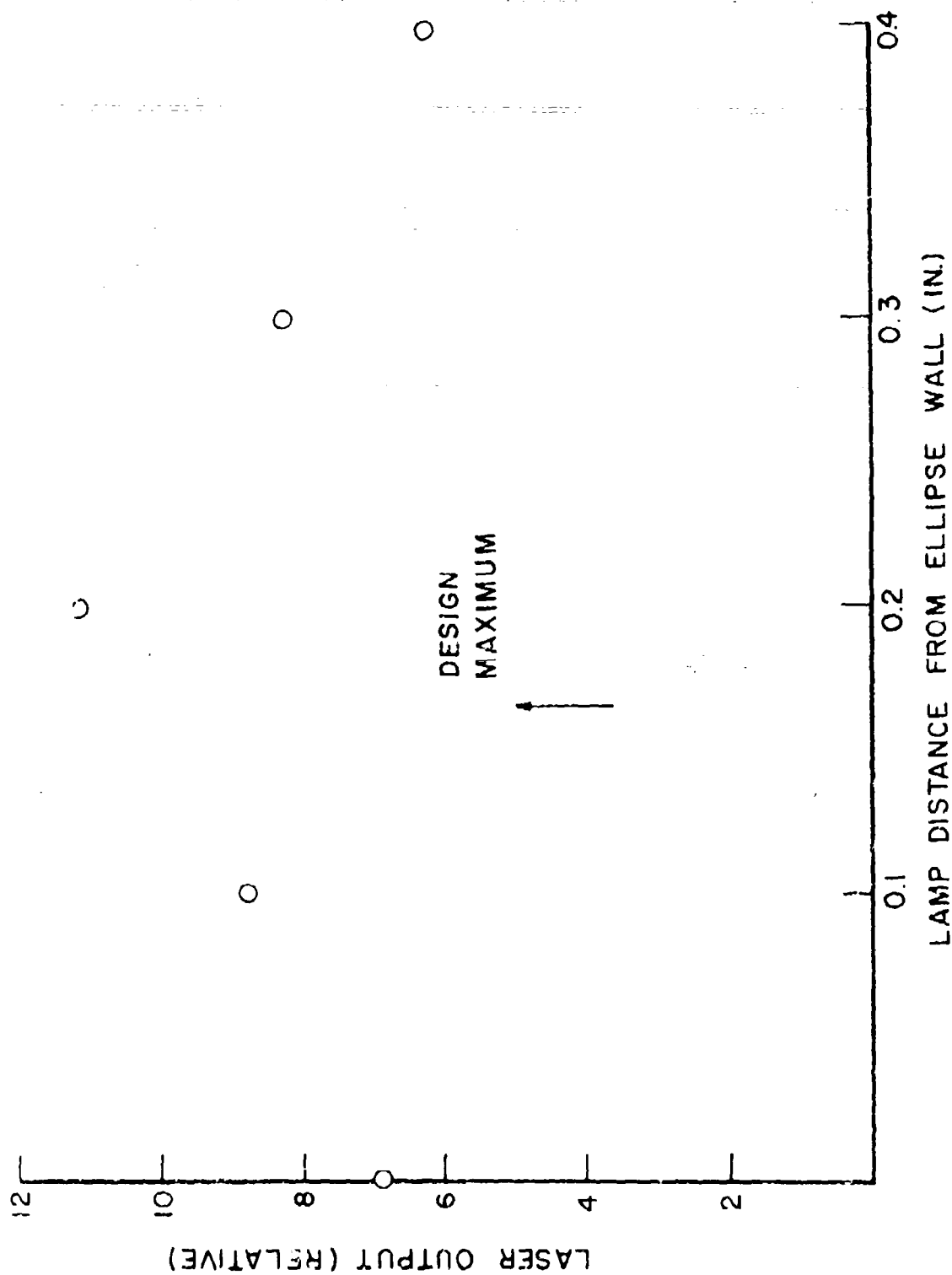
Figure 13. The Variations in Energy Output versus Lamp Position Within the Single Ellipse Cavity. The Laser Rod was Located at One Focus while the Lamp was Moved in 0.1 inch increments from the Opposite Wall through the Other Focus. The Design-Optimum Lamp Position is Indicated.

After optimizing the cavity, threshold was measured using a 922 RCA photodiode and an oscilloscope to detect the laser output. Lasing threshold occurred at a pump lamp input of 90 Joules.

With an input of 250 Joules to the pump lamp the beam divergence was excessive, perhaps as much as several hundred times diffraction limit. This was due to the high degree of optical inhomogenity and generally the poor quality of the rod material. In spite of these facts, the threshold of the system was very low and proved the pump cavity to be an efficient design.

A $Nd:YA\ell O_3$ rod, 3 mm diameter by 30 mm long, was installed in place of the FAP rod and an 85% output coupler added. Threshold for this system, measured as before, was 122 Joules input to the pump lamp. In a pump cavity designed for this size rod a threshold of perhaps 10 Joules would have been expected.

However, in this particular pump cavity the arc volume of the pump lamp exceeded the active material volume by a factor of approximately 10 which indicates that this is also a reasonable threshold when all of the factors influencing threshold are considered.

These experiments have shown that efficient pump cavities can be constructed in house if required.

The following items of equipment and instruments have been assembled within this contract period to facilitate the tasks of laser and SHG materials evaluation.

Two laser heads: one water-cooled double ellipse capable of CW operation with a variety of lamps and laser rod diameters and a second air cooled ellipse described above for pulsed operation. An air cooled ruby system complete with power supply is also available. An extensive selection of pulsed and CW arc lamps filled with xenon and krypton are also on hand. A pulsed power supply has been constructed

entirely with resources available to this contract. The pulsed supply and mechanical Q-switch are shown in Figure 14, connected in a typical configuration. The Q-switch is also of local design and construction. Because this power supply contains several unique features, its operation will be described in some detail in Appendix A. Installation of a closed cycle cooler was undertaken during this contract period but has not been completed. It was found necessary to install additional filters and flow control apparatus to the commercially produced unit. Before the cooling system failures occurred some preliminary data were taken. These tests are described elsewhere in this report. A DC power supply for driving the CW arc lamps are also provided by AFML in conjunction with the cooler and is currently being integrated into the test facility.

Several detectors have also been constructed and tested. The requirements for observing intense sources such as flashlamps and lasers in the visible and near IR is met quite adequately by silicon pin devices and by vacuum photodiodes with S1 and S3 spectral response photocathodes.

These detectors have a very fast time response (less than 1 nsec) and are relatively inexpensive. The vacuum photodetectors are mounted in an arrangement which allows the use of 1-inch diameter filters and lenses and has a variable iris diaphragm and shutter. The output can also be electronically integrated with varous time constants. Load impedences are also selectable from 50 Ω to 1 MΩ. For work in the near IR (out to 3μ) a dewar mounted CdS detector was constructed by UDRI personnel. This detector has a very slow response time (greater than 300 μ sec) and is not suited for the observation of fast pulses. For the measurement of total energy emitted in pulsed observations a calibrated ballistic thermopile was obtained from Hadron, Inc. This device will be useful at pulse energies greater than those which can be measured with the "homemade" calorimeter.

Various adjustable laser mirror mounts have also been fabricated and a versatile table top system of mounting blocks are available to set up

38
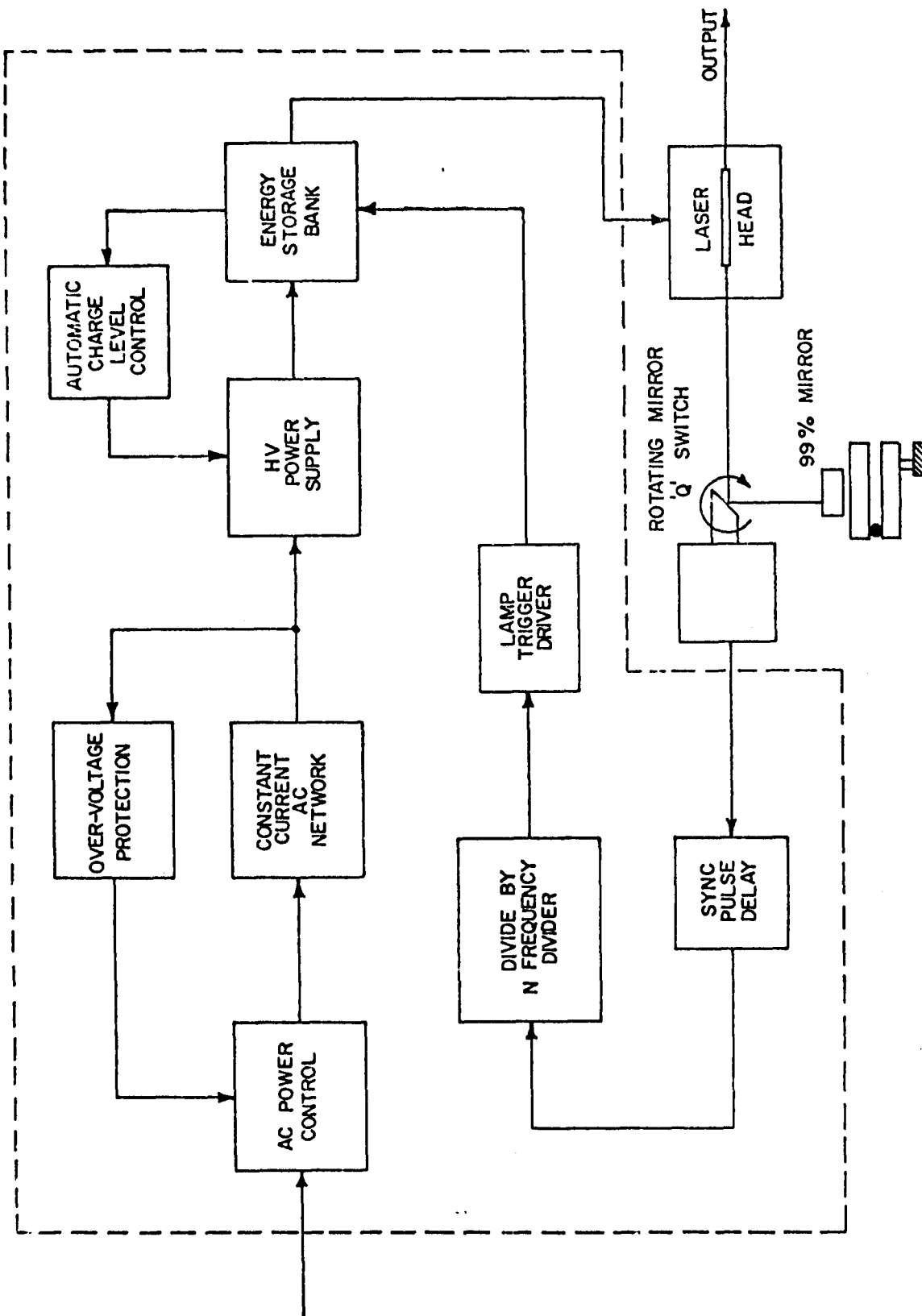
Figure 14. Block Diagram of Pulsed Power Supply. [The Functioning of This Power Supply for Pulsed Supply for Pulsed Laser Operation is Described in the Text. This Block Diagram Shows the General Layout and Interconnections which Allow q-switch Operation, Charge Level Sensing, and Overvoltage Protection.]

39

the materials tests. These fixtures allow rigid mounting of all components to an aluminum toped table made of "Unistrut." The specially constructed table is needed for the most efficient utilization of laboratory space for the location of capacitor banks, pulse forming networks, cooling water circulation equipment, and other utilities.

A temperature controlled oven for the nonlinear optical materials evaluation was also set up and checked out. This item, supplied by AFML, will be incorporated into the test facility as required. Figure 15 shows a block diagram of this set up under development for evaluating nonlinear materials.

4.1 Other Activities

As an amendment to this constract some CO_2 laser work was performed in the spring of 1971 by R. D. Petty and J. A. Detrio. The design, construction, and checkout of the laser and some preliminary studies required diversion of their efforts from the bulk of the work described here. In addition to this special task both men also participated in another research program over an additional period of approximately 6 months. This necessary interruption was in part compensated for by the release of financial resources to purchase some much needed materials and equipment for the materials evaluation facility.

Figure 15. Block Diagram Showing the Nonlinear Materials Test Facility that is Currently Being Integrated into the Laser Materials Evaluation Apparatus. [The Diagram is Somewhat Schematic but Shows the Basic Measurements Desired. The Dotted Outline Indicates the Nonlinear Materials Experiments. The Additional Dispersive Elements and Detectors Required are now Shown.]

SECTION 5

RE-DOPED CdF_2

Cadmium fluoride CdF_2, in its pure form, is an insulator with a 6ev band gap. When it is doped with certain trivalent ions and baked in cadmium vapor at $500^\circ C$, donor-type impurity centers are formed making the material a n-type semiconductor.[31] Reports on electro-luminescence (EL) using this material have been sparse. Light-emitting-diodes (LED's) made from this material doped with either Sm^{3+}, Eu^{3+}, or Tm^{3+} using electrolytic[32] and metallic[33] blocking electrodes have been described. The rather obvious opportunity to develop LED's which emit the characteristic spectra of the RE's is the primary basis for this work with the final goal being to achieve bulk electroluminescence (EL) of such RE-doped samples suitable for use in a laser configuration.

The work accomplished during the contract period consists of the build-up of facilities for sample conversion, surface preparation, electrode application, and EL testing. A preliminary study[34] of the electrical properties of the semiconducting (i. e., converted) samples was completed. The results of this study showed that a metal-insulator-semiconductor (MIS) structure could easily be formed using the converted CdF_2 samples. It also showed that the conductivity which was introduced via a Gd^{3+} impurity, could be reduced by the coaddition of a Ce^{3+} impurity. Effectively, the Ce^{3+} provide a deep trap and thus behaves essentially like a compensator impurity. The studies performed on LED's using samples singly doped with Gd^{3+} show that the EL contains the characteristic spectra of Gd^{3+} at about 2780 and 3120 Å plus a weak, broad-band emission extending from 3000 to 6000 Å. A preprint of a short paper describing these results is given in Appendix B. This paper also provides brief descriptions of the fabrication technique and the interpretation of the observations.

42

Samples containing both Gd^{3+} and Ce^{3+} have also been fabricated into the LED configuration.[35]   The electrical behavior of these LED's are similar to that of the single doped devices with the following exception.   Because of the lower conductivity caused by the Ce^{3+} impurity or, perhaps, due to some additional contribution from this impurity, the double doped samples usually gave higher resistances both in the forward and reverse biased directions but with the reverse-to-forward resistance ratio also higher.

The photoexcited spectra of the double-doped samples shown in Figure 16 are quite different from the Gd^{3+} doped samples.   Besides the Ce^{3+} emission band at around 2900 A, there are many differences in the visible spectra of both the unconverted and converted samples, curves A1, A2, B1, B2, and B3 in Figure 16.   It is apparent that the Ce^{3+} greatly alters the impurity levels in the energy gap.   Finally, the EL spectrum shown in Figure 16, curves C and C', illustrate the most significant difference namely that of a greatly increased blue-white, broad-band output compared to the characteristic emission of Gd^{3+}.   The efficiency of this blue-white emission from the double-doped LED's was increased by at least a factor of 100 over the Gd^{3+} doped devices such that the devices could be operated at 10 to 15 volts dc and be observed in a dimly lighted room.   The Gd^{3+} doped samples had to be pulsed to achieve visually observable light.   The quantum efficiency of the double doped LED's constructed thus far are estimated to be on the order of 0.001 to 0.01%.

The mechanism for the broad-band EL appears, at the present time, to be due to both impact ionization and recombination processes that occur when the mobile electrons (contributed by the Gd^{3+} impurity) interact with the various centers created by the presence of the impurities. Our studies on SrF_2 double doped with Gd^{3+} and Ce^{3+} reported in Section 2 of this report, strongly suggest that the double clusters of Gd^{3+} and Ce^{3+} could be the centers responsible for the observed spectra.   This is supported

49
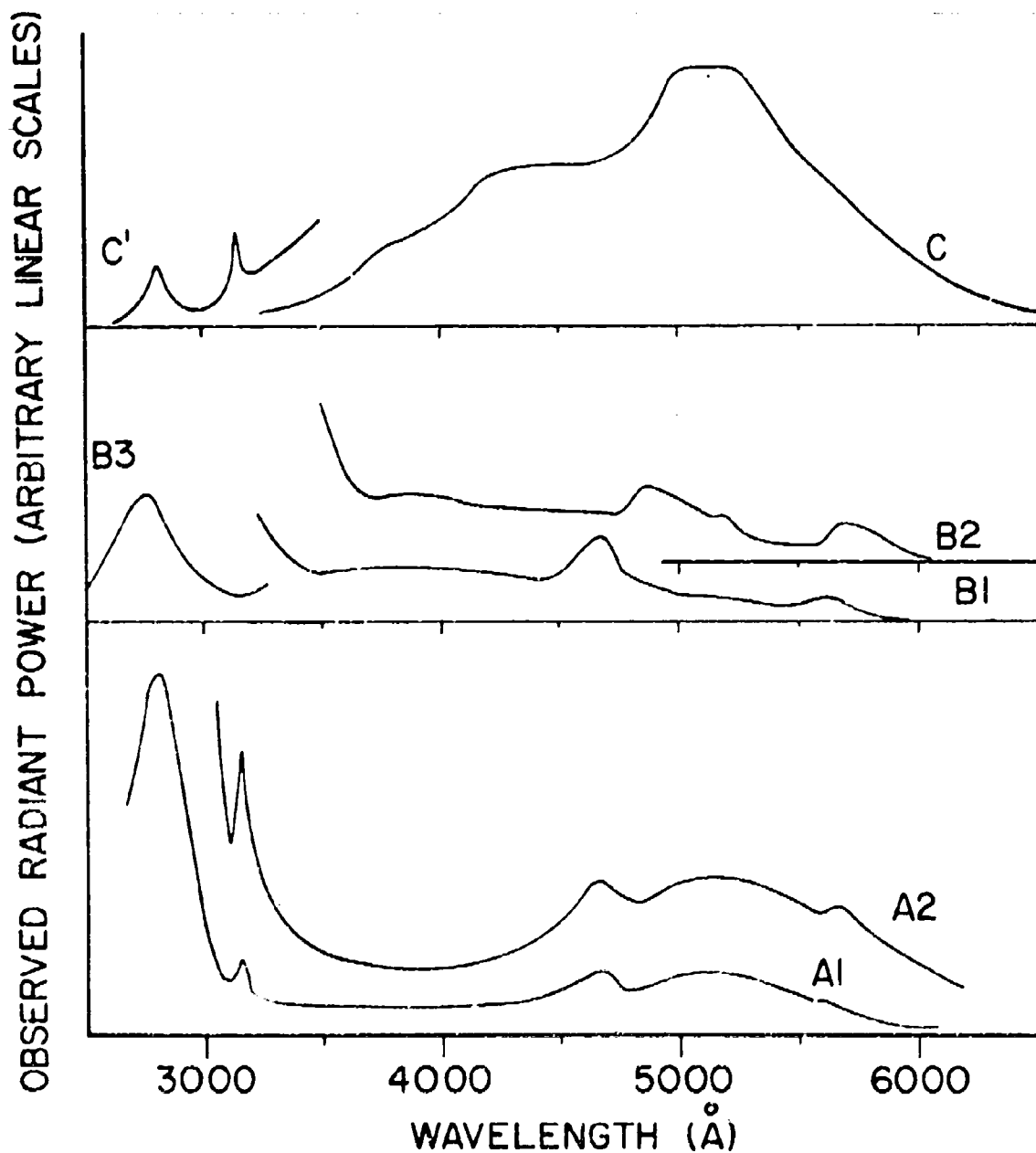
Figure 16. The Room Temperature Fluorescence and Electroluminescence Spectra of Gd³⁺, double doped with Gd³⁺ and Ce³⁺. [Curves A1 and A2 are of the fluorescence spectra of an unconverted (insulating) sample. Curves B1, B2, and B3 are fluorescence spectra of a converted (semiconducting) sample. Curves C and C' are the electroluminescence spectra produced by a LED made from a converted sample. Curves A1 and B1 were obtained using 2500 Å excitation, curves A2 and B2 with 2750 Å excitation, and curve B3 with 2250 Å excitation. Curves C and C' were taken with 5000 and 3000 Å blazed gratings, respectively. The nominal concentrations were 0.02 mole percent Gd³⁺ plus 0.02 to 0.1 mole percent Ce³⁺. The spectra were taken with a 1P28 PM tube and are uncorrected for system response.]

44

somewhat by the fact that the Gd^{3+} absorption spectra of the unconverted double-doped samples shows a complete redistribution of site concentrations with the appearance of a new site spectrum not observed in the single doped samples whose splitting pattern is very similar to the nearest-neighbor doubles spectrum identified in the double doped SrF_2 spectra. Additional indirect evidence for clustering of Ce^{3+} ions with each other and with Gd^{3+} comes from the appearance of a 2900 $\overset{o}{A}$ fluorescence emission. Because of the very nearly equal lattice sizes of CdF_2 and CaF_2, we would expect to see two Ce^{3+} fluorescence bands at wavelengths close to the 3250 and 3450 $\overset{o}{A}$ bands of CaF_2 instead of one band at 2900 $\overset{o}{A}$. Also, according to Loh,[36] Ce^{3+} in tetragonal (C_{4v}) sites of CaF_2 has absorption bands above 2000 $\overset{o}{A}$ at 2050 and 3100 $\overset{o}{A}$. He identifies a cluster band at 2450 $\overset{o}{A}$ which from our studies of double doped SrF_2 has been tentatively assigned to the nearest-neighbor-doubles cluster. In the absorption spectra of Ce^{3+} in CdF_2 we find a strong band at 2480 $\overset{o}{A}$ with two relatively weak bands at 3070 and 2170 $\overset{o}{A}$. Thus, the fluorescence and absorption spectra due to Ce^{3+} strongly suggest that the Ce^{3+} ions, at least, and probably the Gd^{3+} ions are clustering at relatively low concentrations (viz, less than 0.2 mole percent). The blue-white EL, then, would be intimately tied to the energy level scheme of these clusters and to the impurity band structure which would occur at high impurity concentrations.

An invention disclosure describing the applications of this material has been submitted to the sponsor.

SECTION 6

EPR STUDIES

The EPR studies conducted during this work period were concentrated on the SrF_2 and CdF_2 hosts containing Gd^{3+} and Ce^{3+}, both singly doped and together as codopants. The work on the SrF_2 systems was initially motivated by previous optical studies. The goal was to obtain the Ce^{3+} site symmetries in the double doped samples. However, the experiments were inconclusive showing only the expected Ce^{3+} tetragonal spectra and the cubic (O_h), tetragonal (C_{4v}), and trigonal (C_{3v}) spectra of Gd^{3+}. Nevertheless, a detailed analysis[37] of the relative intensities of the Gd^{3+} site spectra showed an anomolous increase of the cubic site concentration. As it turned out, the increase had also been observed in the optical absorption spectra (see Section 2 of this report). A paper[9] was published in which this behavior of the cubic site concentration was tentatively tied to the postulated existence of a local cubic phase. The theoretical basis for such a model of the cubic site is summarized in Section 2 of this report.

The EPR studies of the CdF_2 (Cd^{3+}, Ce^{3+}) system[38] is best summarized by the abstract of the thesis written from these studies.[39]

"The effects of Ce^{3+} doping on the room temperature Gd^{3+} EPR spectra in insulating and semiconducting double doped CdF_2 :0. 02 % Gd^{3+} + 0. x% Ce^{3+} are investigated (0. 006% $\leq$ x $\leq$ 0. 5%). In the insulating crystals, for 0. 006% Ce^{3+} concentration the spectrum is described by a cubic spin Hamiltonian. For the crystal with 0. 02% Ce^{3+} concentration, the spectrum is due to Gd^{3+} in a trigonally distorted environment. The cubic Hamiltonian, with the addition of a very small b_2^0 term describes the spectra. The b_2^0 term is about 1/70 of that which is found for Gd^{3+} in trigonal sites in other fluorite crystals. For 0. 06% Ce^{3+} concentration the spectrum arises from both cubic and weakly trigonally distorted

sites. For the 0.5% Ce^{3+} crystal the spectrum is cubic. Cubic spin Hamiltonian parameters were found for all insulating crystals and in all cases the parameters were within g = 1.991 $\pm$ 0.003; b_4^0 = (47.0 $\pm$ 0.6) x 10^{-4} cm^{-1} and b_6^0 = (0.1 $\pm$ 0.1) x 10^{-4} cm^{-1}. An ad-hoc model is presented to account for these observations.

The spectrum of the semiconducting 0.006% Ce^{3+} crystal consists of seven cubic Gd^{3+} lines and an eighth resonance line that occurs around 32° away from [001]. This is presumably due to exchange interaction between Gd^{3+} ions and trapped electrons that are present as a result of the insulator to semiconductor conversion process. The intensity of the cubic spectrum is about 2% of the intensity of the eighth resonance. The results for the semiconducting 0.02% Ce^{3+} crystal are similar. For the semiconducting 0.06% Ce^{3+} crystal the intensity of the cubic Gd^{3+} spectrum is increased and the intensity of the eighth resonance is decreased indicating a decrease in the number of trapped electrons. This is consistent with the increase of resistivity. The 0.5% Ce^{3+} crystal did not convert to a semiconductor although a number of attempts were made to convert it. The noncubic spectra found in the insulating crystals is not detected in the semiconducting samples. "

SECTION 7

PULSED RAMAN TECHNIQUE

Raman spectroscopy provides information regarding certain vibrations of molecules, solid lattices, and of molecular complexes within solid lattices. In the simplest terms, the vibrating system causes the polarization of the medium to oscillate with very small amplitudes at frequencies that are characteristic of the vibration. Thus, when an electromagnetic wave in the visible range is incident on the medium, it has in the scattered light frequencies which are shifted above and below the incident frequency in addition to the usual unshifted Rayleigh light. These shifted frequencies make up the Raman spectrum.

One of the uses of Raman spectroscopy is the study of the vibrations, usually referred to as local modes, associated with an impurity ion or complex in a crystal. As discussed in Sections 2 and 5 of this report, there is considerable evidence for the claim that clusters of impurity ions in crystals can provide unique and valuable optical and electrooptical properties. Raman spectroscopy coupled with the usual absorption and fluorescence spectroscopy studies can provide a fairly complete picture of the ion placement in the complex. Unfortunately, doped crystals of the type of interest here will produce strong fluorescence emissions when the sample is irradiated with an intense laser beam in a Raman setup. Thus, the observed spectra will usually consist of a rather complicated mixture of Raman and fluorescence spectra.

When it was decided to buildup a Raman facility, it was apparent that a means of discriminating against the fluorescence was required. A review of current Raman techniques[40] indicated that the method of time discrimination against fluorescence was clearly possible but had not been done. This method uses a pulsed laser wherein the duration of

48

pulse is short enough to prevent buildup of the fluorescence emission. Since the response time of a fluorescence emission process is much slower than that of the Raman process, if the photodetector is gated on only during the laser pulse, then the Raman signal will be fully detected while the fluorescence signal will be reduced according to the extent that its response time is greater than the laser pulse length. A paper [41] describing this technique as applied to one particular regime of fluorescence processes has been published. Further details on the technique can be obtained from this paper. An invention disclosure on this technique has been submitted to the sponsor.

SECTION 5

BIBLIOGRAPHY

Technical Reports

M. A. Bafico and P. P. Yaney, "A Preliminary Study of the Electrical Properties of Semiconducting CdF_2 with Ce^{3+} and Gd^{3+} Codopants," Technical Report AFML-TR-72-140 (August, 1972).

D. M. Schaeffer and P. P. Yaney, "Measurement and Analysis of the Fluorescence Decay of Gd^{3+} in SrF_2 versus the Concentration of Codopant Ce^{3+}," Technical Report AFML-TR-72-141 (August, 1972).

Papers Presented

T. P. Graham and G. T. Johnston, "Gd^{3+} EPR in Ce^{3+} - Gd^{3+} Doubly Doped SrF_2," Bull. Am. Phys. Soc. 16, 360 (1971).

P. P. Yaney, "Calculation of the Electrostatically Correlated Crystal Field Interaction for Gd^{3+}:MeF_2," Bull. Am. Phys. Soc. 16, 447 (1971).

M. A. Bafico and P. P. Yaney, "Electrical and Optical Properties of Semiconducting CdF_2 (Ce^{3+} + Gd^{3+})," Bull. Am. Phys. Soc. 16, 856 (1971).

G. K. Miner, J. B. Pastora, G. T. Johnston, and T. P. Graham, "Gd^{3+} EPR in Ce^{3+} - Gd^{3+} Doubly Doped Semiconducting CdF_2," Bull. Am. Phys. Soc. 16, 857 (1971).

J. B. Pastora, G. K. Miner, G. T. Johnston, and T. P. Graham, "Gd^{3+} EPR in Ce^{3+} - Gd^{3+} Doubly Doped Insulating CdF_2," Bull. Am. Phys. Soc. 16, 857 (1971).

P. P. Yaney and D. M. Schaeffer, "Excitation and Decay Modes for Fluorescence Transitions from the $^6P_{7/2}$ Manifold of Gd^{3+}:SrF_2(Ce^{3+})," Bull. Am. Phys. Soc. 17, 130 (1972).

T. P. Graham, G. K. Miner and G. T. Johnston, "Low Temperature EPR Studies in SrF_2:(Gd^{3+}, Ce^{3+})," Bull. Am. Phys. Soc. 17, 130 (1972).

J. H. O'Hare, "A Model For a Cubic Phase in SrF_2:(Gd^{3+}, Ce^{3+}) With Local Charge Compensation," Bull. Am. Phys. Soc. 17, 130 (1972).

G. K. Miner, T. P. Graham and G. T. Johnston, "Intensity Studies of Gd^{3+} EPR in SrF_2 vs. Ce^{3+} Concentration," Bull. Am. Phys. Soc. 17, 185 (1972).

P. P. Yaney, "Raman Studies Using a Q-Switched Nd:YAG Laser in Burst Mode - A Preliminary Report," Bull. Am. Phys. Soc. 17, 186 (1972).

50

G. T. Johnston, J. B. Pastora, G. K. Miner, and T. P. Graham, Intensity Studies of Gd^{3+} EPR in CdF_2 as a Function of Ce^{3+}, a Second Dopant," Bull. Am. Phys. Soc. <u>17</u>, 201 (1972).

G. T. Johnston, T. P. Graham, and G. K. Miner, "NMR Calibration of an EPR Field Marker," Proceedings of the Kentucky Academy of Science (1972).

Publications

J. M. O'Hare, "Calculations of the Spectra of $SrF_2:Gd^{3+}$ in a Tetragonal Crystal Field," Phys. Rev. <u>B3</u>, 3603 (1971).

G. K. Miner, T. P. Graham, and G. T. Johnston, "Effect of a Ce^{3+} Codopant on the Gd^{3+} EPR Spectrum of SrF_2 at Room Temperature," J. Chem. Phys. <u>57</u>, 1263 (1972).

G. K. Miner, T. P. Graham, and G. T. Johnston, "The Preparation and Calibration of a Convenient EPR Marker and Intensity Reference," Rev. Sci. Instr. <u>43</u>, 1297 (1972).

J. M. O'Hare, "Model for Locally Compensated Cubic Sites of Tripositive Rare Earth Ions in Fluorite Crystals," J. Chem. Phys. <u>57</u>, 3838 (1972).

P. P. Yaney, "Reduction of Fluorescence Background in Raman Spectra by the Pulsed Raman Technique," J. Opt. Soc. Am. <u>62</u>, 1297 (1972).

J. A. Detrio, "Normalized Legendre Functions and Tesseral Harmonics of 7th Order", J. Chem. Phys. <u>57</u>, 5012 (1972).

REFERENCES FOR PART I

1. J. A. Detrio, M. W. Ferralli, P. P. Yaney, D. M. Ware, and V. L. Donlan, J. Chem. Phys. 53, 4372 (1970), and M. W. Ferralli and P. P. Yaney, Technical Report AFML-TR-69-318 (March, 1970), USAF Materials Laboratory, Wright-Patterson Air Force Base.

2. A. H. Piksis, G. H. Dieke, and H. M. Crosswhite, J. Chem. Phys. 47, 5083 (1967).

3. G. H. Dieke and L. Leopold, J. Opt. Soc. Am. 47, 944 (1957), and K. H. Hellwege, S. Hufner, and H. Schmidt, Z. Physik 172, 460 (1963).

4. S. P. Cook and G. H. Dieke, J. Chem. Phys. 27, 1213 (1957).

5. G. S. Ofelt, J. Chem. Phys. 37, 511 (1962).

6. B. R. Judd, Phys. Rev. 127, 750 (1962).

7. Due to J. A. Detrio.

8. Due to P. P. Yaney.

9. G. K. Miner, T. P. Graham, and G. T. Johnston, J. Chem. Phys. 57, 1263 (1972).

10. D. M. Schaeffer and P. P. Yaney, Technical Report AFML-TR-72-141 (August, 1972), USAF Materials Laboratory, Wright-Patterson Air Force Base and Bull. Am. Phys. Soc. 15, 849 (1970).

11. J. L. Wolf and P. P. Yaney, Technical Report AFML-TR-69-232 (August, 1969), USAF Materials Laboratory, Wright-Patterson Air Force Base.

12. J. M. O'Hare, J. Chem. Phys. 57, 3838 (1972).

13. J. M. O'Hare, Bull. Am. Phys. Soc. 17, 130 (1972).

14. P. P. Yaney and D. M. Schaeffer, Bull. Am. Phys. Soc. 17, 130 (1972).

15. M. M. Kreitman and D. L. Barnett, J. Chem. Phys. 43, 364 (1972).

16. N. Kristianpoller and Y. Kirsh, Phys. Rev. B. 4, 635 (1971).

17. R. H. Heist and F. K. Fong, Phys. Rev. B. 1, 2970 (1970).

18. J. A. Detrio, J. Chem. Phys., $\underline{57}$, 5012 (1972).

19. K. Rajnak and B. G. Wybourne, Phys. Rev. $\underline{132}$, 280 (1963).

20. K. Rajnak, J. Opt. Soc. Am. $\underline{55}$, 126 (1965).

21. B. R. Judd, Phys. Rev. $\underline{141}$, 4 (1966).

22. B. R. Judd, H. M. Crosswhite, and Hannah Crosswhite, Phys. Rev. $\underline{169}$, 130 (1968).

23. K. Rajnak and B. G. Wybourne, Phys. Rev. $\underline{134}$, A596 (1964).

24. J. M. O'Hare, Phys. Rev. $\underline{B3}$, 3603 (1971).

25. J. Makovsky, J. Chem. Phys. $\underline{46}$, 390 (1967).

26. F. Z. Gilfanov, L. D. Livanova, A. L. Stolov, and Ya. P. Khodyrev, Opt. Spectrosk. $\underline{23}$, 431 (1967) [translation: Opt. Spectrosc. $\underline{23}$, 231 (1967)].

27. J. M. O'Hare and V. L. Donlan, Phys. Rev. $\underline{185}$, 416 (1969)

28. P. P. Yaney, Bull. Am. Phys. Soc. $\underline{15}$, 849 (1970).

29. K. Rajnak and B. G. Wybourne, J. Chem. Phys. $\underline{41}$, 565 (1964).

30. P. P. Yaney, Bull. Am. Phys. Soc. $\underline{16}$, 447 (1971).

31. J. D. Kingsley and J. S. Prener, Phys. Rev. Letters $\underline{8}$, 315 (1962).

32. J. Lambe, D. K. Donald, W. C. Vassell, and T. Cole, Appl. Phys. Letters $\underline{8}$, 16 (1966).

33. B. S. Skorobogatov, M. F. Dubovik, V. V. Azarov, and L. B. Kolner, Opt. Spektrosk. $\underline{22}$, 981 (1967) [translation: Opt. Spectrosc. $\underline{22}$, 534 (1967)].

34. M. A. Bafico and P. P. Yaney, Technical Report AFML-TR-72-140 (August, 1972), USAF Materials Laboratory, Wright-Patterson Air Force Base, and Bull. Am. Phys. Soc. $\underline{16}$, 856 (1971).

35. P. P. Yaney and M. A. Bafico, Bull. Am. Phys. Soc. $\underline{18}$, to be published (1973).

36. E. Loh, Phys. Rev. $\underline{154}$, 270 (1967).

37. T. P. Graham and G. T. Johnston, Bull. Am. Phys. Soc. $\underline{16}$, 360 (1971).

38. J. B. Pastora, G. K. Miner, G. T. Johnston, and T. P. Graham, Bull. Am. Phys. Soc. $\underline{16}$, 857 (1971); See also G. K. Miner, J. B. Pastora, G. T. Johnston, and T. P. Graham, ibid.

39. J. B. Pastora, "An EPR Investigation of Gd^{3+} in Insulating and Semi-conducting CdF_2 Containing Ce^{3+} as a Codopant," M. S. Thesis (University of Dayton, 1971).

40. P. P. Yaney, Departmental Report on Light Scattering Summer School, Northwestern University held July 20-31, 1970 (September 1970), unpublished.

41. P. P. Yaney, J. Opt. Soc. Am. 62, 1297 (1972).

APPENDICES FOR PART I
APPENDIX A

POWER SUPPLY OPERATION

The power supply built for repetitive pulsed operation is capable of delivering a constant current of 150 mA at up to 5 KV. The charging control (voltage setting) and constant current feature are made possible by the use of an AC constant current network on the main input to the supply. This resonant circuit is tuned so that when the control triac is fired the series resonance produces a very high impedance to the input and no current flows in the primary of the high voltage transformer. This arrangement works well because a solid state device such as the triac can be switched to a conducting state readily, whereas interrupting the flow of current with such a device in series with the line can be less reliable and usually requires more "drive." The output of the high voltage transformer is full-wave rectified and is used to feed the capacitive storage bank. The output of the bridge is also shunted by a high resistance voltage divider to allow the voltage level to be sensed by op-amp circuits which control the firing of the triac. A number of safety interlocks also control the firing of the triac and an additional relay controlled storage bank dump.

The firing of the lamp is controlled in several modes: 1) free-running pulsed operation controlled by a variable frequency pulse generator, 2) single s' - Q switched and long mode operation, and 3) repetitively operated Q-switched operation. The flashlamp pulses are synchronized with the location of the mechanical Q-switch by means of a synchronous pulse generated at the rotating mirror by a magnetic pickup. These pulses are fed into a digital logic circuit which allows them to be counted down from 15000 ppm to a repetition rate within the capability of the flashlamp and power supply. The timing pulses are amplified and used to drive the series injection trigger circuit (EG&G model 146A).

A similar sequence is followed in the single-shot case but only one pulse is generated. In the "long mode" operation the Q-switch is not used. The complete design contains additional features which are required for operation but which are not essential for explaining the principles of operation.

APPENDIX B

ELECTROLUMINESCENCE OF Gd^{3+}-DOPED CdF_2 IN A LIGHT-EMITTING DIODE*

Perry Pappas Yaney and Michael A. Bafico
Department of Physics, University of Dayton

ABSTRACT

Light-emitting diodes were fabricated using CdF_2 (0.02% Gd^{3+}) which had been converted to the n-type semiconducting state by heating in cadmium vapor. The electroluminescence was observed at the negatively-biased blocking electrode with 5 to 15 volts applied. The emitted light consisted of the expected characteristic near-uv spectra of Gd^{3+} (2780 and 3120 Å) and a previously unreported 3000 Å wide band centered at about 4500 Å. The nearly-white emission was sufficient to be seen in a dimly lighted room and the radiant power output had an approximate cubic dependence on the diode current. The observations were made at room temperature.

TEXT

In 1962 Kingsley and Prene reported that normally insulating CdF_2, which was doped with certain trivalent ions, could be converted to a n-type semiconducting state by heating in cadmium vapor at about $500^{\circ}C$. Since that time, numerous papers[2] have appeared directed primarily at the electrical and optical properties of this interesting material. The trivalent ions most often used to effect conversion are certain members[3] of the rare earth series. The attractive possibility of electrical excitation of the characteristic fluorescence spectra of these ions in a solid was reported[4,5] for Sm^{3+}, Eu^{3+}, and Tb^{3+} from the negatively-biased blocking electrode of a two-terminal device using semiconducting CdF_2 as the intervening medium. The purpose of this letter is to report additional observations on CdF_2 light-emitting diodes (LED's) using Gd^{3+} as the dopant.

Gadolinium is unique among the rare earth series in that its only fluorescence emission is in the near-uv and originates from the ^6I manifold of crystal field levels around 36,000 cm^{-1} (2780 Å) and the ^6P manifold around 32,000 cm^{-1} (3120 Å).[6] The terminal levels for these transitions and the only levels below the ^6P group are those of the ^8S ground state. Converted

samples of Gd^{3+} doped CdF_2 have a blue color whereas the unconverted sample is colorless. The color is due to a strong infrared absorption band, the short wavelength wing of which produces absorption in the red portion of the visible region. This band has been identified as being due to the ionization of electron traps.[3,7]

The LED's reported on herein have one ohmic electrode using ultrasonically soldered indium and the remaining electrode of the blocking type using usually either vacuum evaporated indium or silver. The reverse-to-forward resistance ratios are on the order of 100. The electroluminescence (EL) is observed at the blocking electrode when it is negative. Typically, converted samples containing a nominal Gd^{3+} concentration of 0.02 mole percent have resistivities between 0.1 and 1 ohm-cm at room temperature. Figure B.1 shows the various observed spectra. Curve A is the weak photo-excited fluorescence spectrum of the pure CdF_2 single crystal obtained from Optovac.[8] All samples were grown using 99.999 percent pure CdF_2 from General Electric Chemical Products Plant.[9] Curve B is the strong photo-excited spectrum of the unconverted Gd^{3+} doped CdF_2 crystal. The sharp line is from the $^6P_{7/2}$ state of Gd^{3+}. The broad fluorescence band centered at 5250 $\overset{o}{A}$ is not unique to gadolinium doped samples in that this band is either weakly present in the spectra of our other rare-earth doped CdF_2 samples or it is a dominate feature (e.g., Nd^{3+}). Only the lines characteristic of Gd^{3+} appear in the absorption spectrum. Curve C shows the drastic effect the conversion process has on the 5250 $\overset{o}{A}$ band and the gadolinium emission. Curve D is the spectrum of the EL. The four curves are uncorrected for photomultiplier response (1P28) and spectrometer efficiency. The three photoexcited curves were obtained using a source about 150 $\overset{o}{A}$ wide centered on 2750 $\overset{o}{A}$. The EL spectrum shows the expected characteristic uv-line spectra of Gd^{3+} and, in addition, a nearly white-light emission. The brightness of the white EL from these devices was sufficient to be seen in a dimly lighted room. The source of such a broad band of emission can be attributed to a distribution of traps in the 6 eV band gap, produced by Gd^{3+} and/or some trace impurity, to lattice defects, or to a combination of these.
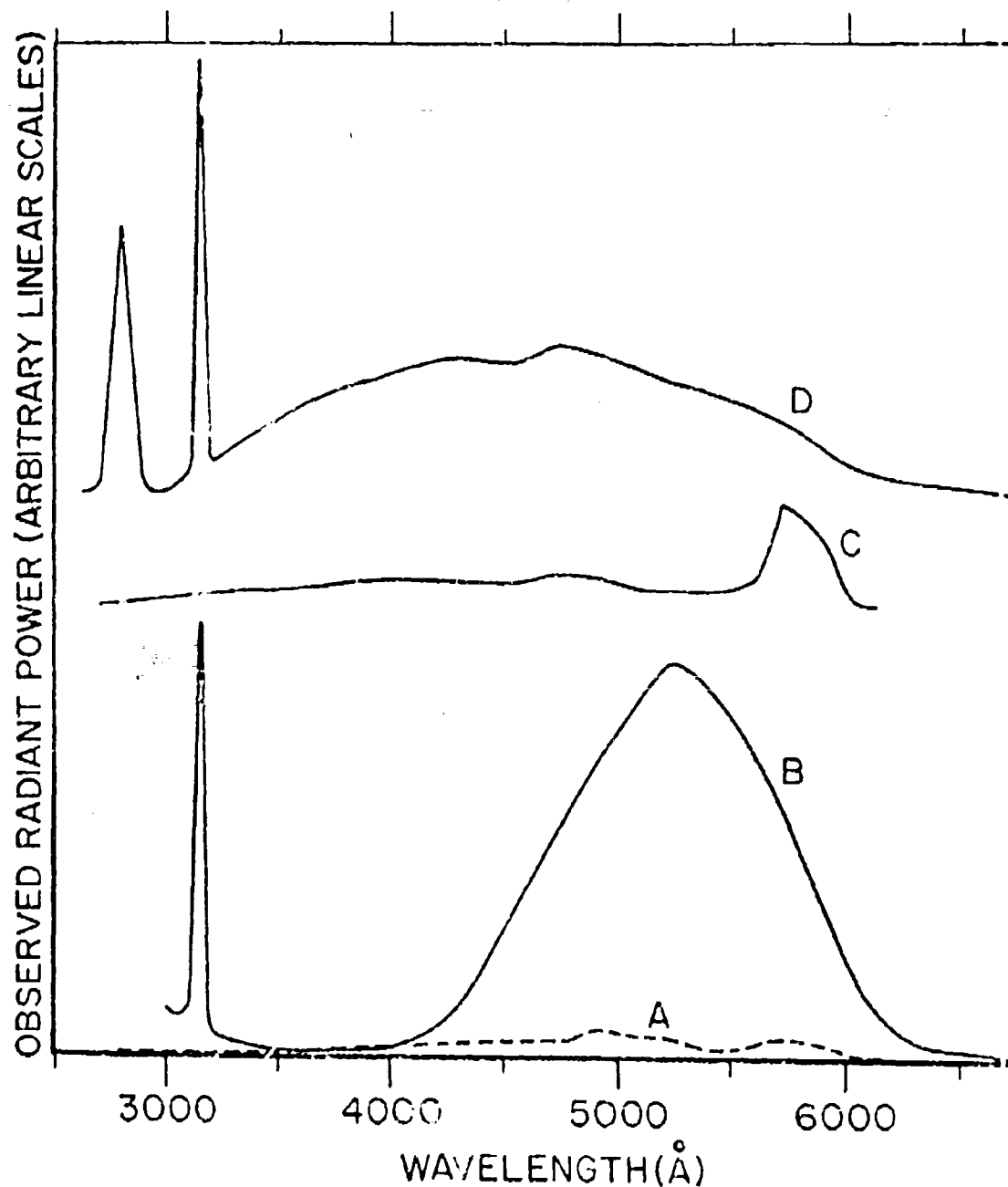
Figure B.1, Emission Spectra Observed at Various Stages of Fabricating a CdF_2 (Gd^{3+}) LED. Curves A, B, and C are Photoexcited Using 2750 Å excitation. Curve A is From a Pure Undoped CdF_2 Sample. Curve B is From An Unconverted Gd^{3+}-doped Sample. Curve C is From a Converted (i. e., Semiconducting) Gd^{3+}-Doped Sample. Curve D is the Electroluminescence Spectrum from a Pulsed LED.

The broad near-gaussian-shaped fluorescence band shown in Curve B has its excitation band centered at 2900 $\overset{o}{A}$ and with about half the width of the fluorescence band. These features[10] suggest that this band comes from a lattice defect (i.e., a color center) concentration which was increased by the addition of the trivalent impurity to the divalent host. In Curve C, we see that both this band and the Gd^{3+} emission are missing. Since the end result of the conversion process is the replacement of the interstitial F^- ions (which compensated the additional charge on the rare-earth impurity ion) by lattice electrons, one explanation is that this broad band is an excitation of the interstitial F^- ion.[3] A reduction of the characteristic emission of Gd^{3+} would be expected due to greatly increased coupling to the lattice due to the lattice electrons (i.e., polarons) thereby lowering the quantum yield of the fluorescence.

Both pulsed (usually 1 ms at 1 to 20 Hz) and dc measurements were made on these LED's. Electroluminescence was observed to occur at the same relatively well-defined voltage for a given device regardless of whether pulse or dc excitation was used. This voltage ranged from 5 to 15 volts depending on the surface preparation and details of the fabrication. The dc current-voltage (I-V) curves show ohmic behavior at low currents followed by an approximate V^2 dependence suggesting a space-charge-limited current regime. The end of this regime occurs with the onset of the light emission. The diode is at its breakdown voltage at this point and the radiant power output P increases with current I according to $P \propto I^n$ where $n \approx 2.5$ to 3. An $\exp(a/V^{1/2})$ dependence can be fitted to the P-V data which is consistent with the impact ionization process in a Schottky-type barrier.[11] This process is usually suggested with n-type material when the EL is observed at the negatively-biased blocking electrode.[12] However, the dynamic range over which the radiant power was measured was insufficient to make this fit unique. The range was limited due to device heating to about a decade in the pulsed measurements and to about one half decade in the dc measurements.

In summary, we have observed the predictable uv-line emission plus an unexpected nearly-white light emission from Gd^{3+}-doped-CdF_2 LED's at room

temperature with the radiant power having an approximate cubic dependence on current. The EL mechanism for these devices appears to be that of impact ionization occurring in the reverse-bias breakdown regime of the diode.

REFERENCES

1. J. D. Kingsley and J. S. Prener, Phys. Rev. Letters 8, 315 (1962).

2. See, for example, the paper by T. H. Lee and F. Moser, Phys. Rev. B 3, 347 (1971) and the references cited therein.

3. P. F. Weller, Inorganic Chem. 4, 1545 (1965).

4. J. Lambe, D. K. Donald, W. C. Vassell, and T. Cole, Appl. Phys. Letters 8, 16 (1966).

5. B. S. Skorobogatov, M. F. Dubovik, V. V. Azarov, and L. B. Kolner, Opt. Spektrosk. 22, 981 (1967) translation: Opt. Spectrosc. 22, 534 (1967) .

6. G. H. Dieke and L. Leopold, J. Opt. Soc. Am. 47, 944 (1957).

7. F. Moser, D. Matz, and S. Lyer, Phys. Rev. 182, 808 (1969).

8. Optovac, Inc., North Brookfield, Mass. 01535. The pure CdF_2 material used in this work has an optical density difference of 0.26 between 4000 and 2200 Å for a 1.9 mm sample.

9. General Electric Chemical Products Plant, 1099 Ivanhoe Road, Cleveland, Ohio 44110.

10. W. Beall Fowler, in Physics of Color Centers, edited by W. Beall Fowler. (Academic Press, New York, 1968), pp. 54-61.

11. G. F. Alfrey and J. B. Taylor, Brit. J. Appl. Phys. 4, 544 (1955).

12. A. G. Fischer in Luminescence of Inorganic Solids, edited by P. Goldberg. (Academic Press, New York, 1966), pp. 580-585.

PART II

ELECTRICAL AND OPTICAL PROPERTIES OF
SEMICONDUCTING MATERIALS

Dr. Rex L. Jones

INTRODUCTION

This work was concerned with research and development on the electrical
and optical properties of semiconducting materials. The effort encompassed
material preparation, determination of electrical and optical properties, design
and construction modification of specialized equipment required for these
investigations, and the compilation of papers available in the open literature.

SECTION 9

ELECTRICAL AND OPTICAL PROPERTIES OF
SEMICONDUCTING MATERIALS

9.1 ELECTRICAL PROPERTIES OF DEFECT CENTERS IN SEMICONDUCTORS

Transport and electrical properties were measured on II-VI compounds
with a variety of dopants and after a variety of heat treatments in order to
determine those procedures with the best potential for application in obtaining
optoelectronic devices. Research was also conducted to obtain reliable ohmic
contacts to these crystals.

The electrical measurements were comprised mainly of guarded Hall and
guarded Van der Pauw measurements versus temperature, T, and resistivity
or conductivity versus temperature, both over the same temperature range.
The raw data from these measurements was feed into the computer at Wright-
Patterson Air Force Base using programs developed by Air Force Materials
Laboratory (AFML) personnel to obtain compilation and plots of charge carriers
per cubic centimeter, conductivity and mobility versus $1/T$. The temperature
range covered by some of these measurements were from liquid helium to 52°C.
Some photo-Hall measurements on these II-VI compounds were also performed.

Materials studied during the contractual period were ZnSe, 0.01% Li;
ZnSe, 0.1% Li; ZnSe, 0.001% Cu; ZnSe (Na); ZnSe, implanted with Zn; ZnO,
hydrothermally grown with Li; CdS; and ZnS.

A typical heat treatment consisted of sealing the sample or samples along with the doping element or substance surrounding vapor upon heat which forms filling with helium gas after evacuation and purging with nitrogen gas. The capsule was then placed in a furnace with a long flat heat zone at nominally 1000°C for a time varying from hours to 10 days. The sample was then removed and its transport and/or electrical properties were measured over a temperature range or at several discrete temperatures. Analysis of the computer output was then done to determine the course of the continuing experimentation.

Ohmic contact studies to these II_B-VI_B compounds were conducted using soldering and sputtering techniques. Soldering techniques were not attempted to p-type material, except in an attempt to produce a p-n junction. Prior to forming the contact, the sample was etched or cleaned using acetone, deionized water and alcohol. Sputtering of Cu, Pt, and Au to ZnSe, ZnO, CdSe and CdS was attempted at one point or other with the sputtered Au seeming to form the preferred contact. Acceptable ohmic contact were made to ZnO using indium solder followed by a heat treatment. The acceptability of the contacts were checked using I/V or C/V measuring equipment.

During the contractual period, among the items fabricated were: stand for new Veeco ion vacuum pump, front surface mirror for mounting right angle source, circuit box to facilitate I/V characterization of samples, sputtering system for contacting the semiconducting material, and a new sample holding system containing four phosphorus bronze spring fingers to hold the Van der Pauw sample against the beryllium oxide substrate. Among the items modified were: the heater in the helium dewar system and the rewiring of the Hall measuring dewar to increase the facilities to include Van der Pauw measurements. Among the equipment assembled, installed, and checked out to manufacture specifications were: diamond wire saw, transistor curve tracer, isolation transformer in Hall measuring equipment, furnace to obtain flat heat zone, and isothermal furnace.

OPTICAL PROPERTIES OF DEFECT CENTERS IN SEMICONDUCTORS

The main thrust of the optical studies has been directed at annealing studies between 300°C and 600°C of radiation-induced photoluminescence bands in germanium, absorption measurements of radiation damaged silicon at liquid nitrogen and liquid helium temperature, and comparsion studies between photo- luminescence experiments and absorption experiments on electron radiation damaged silicon. Photoluminescence measurements of germanium samples were made using first a conventional infrared source and after acquisition by AFML, a NdYAG laser in both continuous and pulsed mode as the exciting source of radiation. Time constant measurement were also made on these photo- luminescence peaks using the NdYAG laser. It was not possible to make photo- luminescence measurements of silicon samples using the NdYAG laser as the source of exciting radiation, since the transitional energy involved in the lasering transition is less then the band gap of silicon at liquid helium temperature. Thus, the absorption of the lasing radiation from the NdYAG laser for silicon is small.

Experiments were conducted to determine the laser power output versus laser lamp power for various pulsed modes of operation, to determine the type of chopper and chopper blade to use in making time constant measurements while using a continuous source as the exciting source of radiation, and to determine the time constant of the newly acquired InSb and InAs detectors while at their operating temperature of 77°K.

Three new gratings; 295 grooves/mm blazed at 2. 6μ; 590 g/mm, 1. 3μ; 590 g/mm, 2. 1μ; were calibrated versus wavelength and had response corrections factors determined for them. The 590 groove/mm grating blazed at 2. 1μ was found to be incorrectly blazed and was returned. The response correction factor is used to normalized the photoluminescence intensity versus wave- length to that of a blackbody at a given temperature. It is obtained by replacing the photoluminescence sample by a blackbody source and measuring its spectral response. The photoluminescence data can then be converted to photon flux versus wavelength.

The photoluminescence and optical absorption data were first recorded on strip chart recorder charts. The response at a given wavelength and the wavelength were read from these charts and punched on computer cards to provide a data deck. This data deck and the particular program were then entered into the computer for computation and compilation. After computation and compilation, the results are plotted using a Cal-Comp plotter.

These programs have been modified to run on either a Com-Share terminal, the IBM-7094, or the present CDC 6600. The Cal-Comp plotter is not connected to the Com-Share terminal, thus Cal-Comp results are not obtainable directly from it. The program allows parameters to be varied such that plots suitable for journal reports are obtainable.

Besides these programs, programs have been written that will calculate the photon flux at a given wavelength from a blackbody at a given temperature and will determine the slope of a computer determined least square fit to a set of data points. Other programs were written and assistance was given to other personnel in writing and modifying their computer programs.

During the contractual period, among the items fabricated were: infrasil and suprasil windows for the liquid helium dewar using the diamond wire saw; optical filters from single crystal silicon by cutting on a diamond circular saw, polishing with diamond paste to 1μ finish, and final shaping using a diamond wire saw; a diamond crystal model to represent either silicon or germanium with placing other atoms and bonds in it to show the vacancies, substitutions and interstitials that occurs in these crystalline semiconductors; brass clamps to hold the liquid helium dewar to its mounting plate allowing the dewar to be placed upside down to facilitate the draining of water that condenses during an experiment, pumping station, and the samples used in the photoluminescence and absorption studies from boules of silicon and germanium. Among the items assembled and intalled were: a blackbody source to check the rise in temperature versus time to ascertain that the specifications were met; a Nd YAG, 10 watt laser from Quantronix; a optical bench received from

65

surplus; the electronics, power supply, temperature controller, strip chart recorder and shelf, to measure and control the sample temperature in a cryogenic dewar; and a thermocouple on or near the sample for temperature measurements. This thermocouple attachment proved inadequate and a cryogenic diode was purchased which required modification of electronic connections on the research helium dewar. The helium research dewar was also modified so the sample holder would vertically align better with the optical holder.

Early in the contractual period plans for incorporation of a data acquisition system on the Czerny-Turner spectrometer used in photoluminescence were discussed. The mechanical and electronic components necessary to digitize the spectrometer were ordered, assembled and installed. The data acquisition system itself is mounted on a movable rack such that it is useable by other experimenters and consists of a digital voltmeter with BCD output, a HP 2570A coupler/controller and a high speed paper-tape punch.

All during the contractual period a literature search for pertinent journal and periodical articles, followed by xeroxing and author indexing on 3 x 5 cards was conducted.

PART III

INTRINSIC COERCIVE FORCE IN MULTIDOMAIN SINGLE CRYSTAL (RARE EARTH) Co_5 ALLOYS

Dr. Clark W. Searle[*]

INTRODUCTION

This part dealt with an intrinsic coercive force in the magnetic characteristics of several RCo_5 (R is a rare earth element) alloys prepared as single crystals by the Battelle Columbus Laboratories. The experimental data is shown to lead to a model which consists of a periodic pinning structure with a period about an order of magnitude larger than that of the crystal lattice.

SECTION 10

INTRINSIC COERCIVE FORCE IN MULTIDOMAIN SINGLE CRYSTAL (RARE EARTH) Co_5 ALLOYS

10.1 INTRODUCTION

Most previous investigations of the coercive force, H_c, associated with RCo_5 alloys, have analyzed small particle hysteresis loops[1] where domain wall nucleation is often dominated by surface conditions. It has recently been suggested that large domain wall energies may be related to the high H_c for $SmCo_5$.[2] Other studies have shown that high energy narrow domain walls can lead to an H_i related to the periodicity of the lattice.[3,4] The purpose of this work was to study H_i by applying the external field, H, in the easy direction of relatively large multidomain single crystal spheres, where bulk properties dominate. The expected effect is shown in Figure 17b.

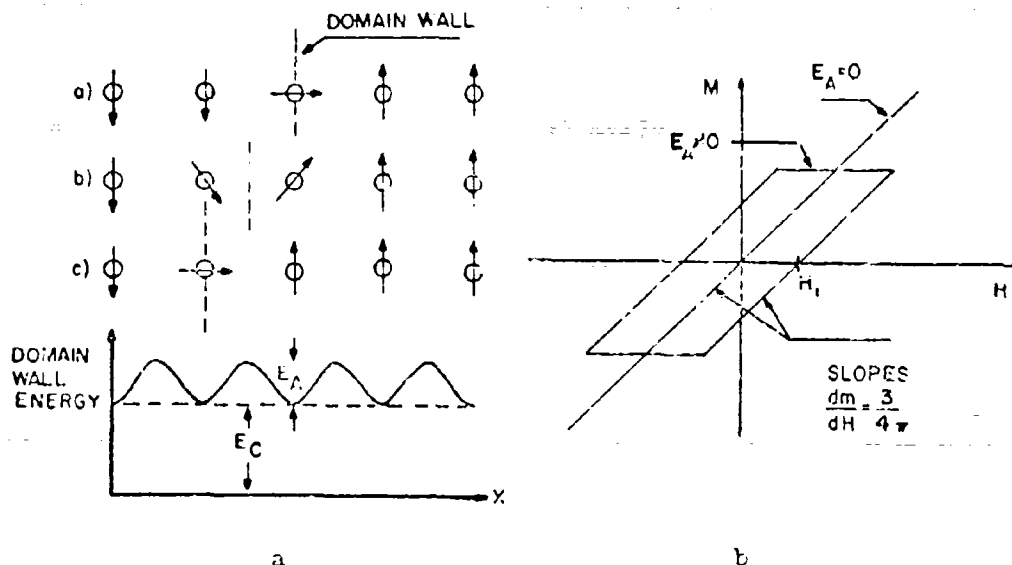[*] On leave from the University of Manitoba, Winnipeg, Manitoba, Canada.

Figure 17. Hysteresis Loop Associated With a Periodic
Fluctuation in Domain Wall Energy

This effect would be related to the periodic flucuations in domain wall energy shown in Figure 17a, and has apparently been observed in an aligned powder.[5] All the data was obtained using a variable temperature Princeton Applied Research VSM. H was swept linearly and the hysteresis loops were recorded on an x-y recorder.

10.2 EXPERIMENTAL RESULTS

Typical room temperature results are shown in Figure 18. H was varied at a rate of 100 oe/min. Room temperature values for H_i are 16 Oe($SmCo_5$) and 4 Oe(YCo_5). $NdCo_5$ and Ni were also measured under identical conditions with $H_i = 0$. These curves have been omitted for clarity.

The temperature dependence of H_i is indicated in Figure 19. H_i is linearly dependent on T, with a negative slope, over most of the temperature range.
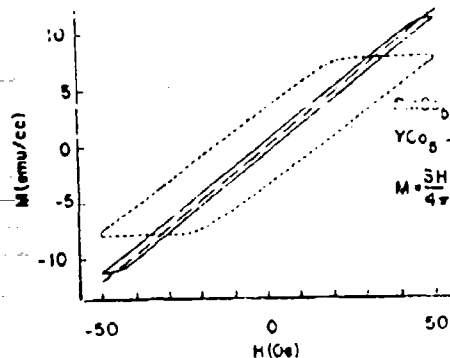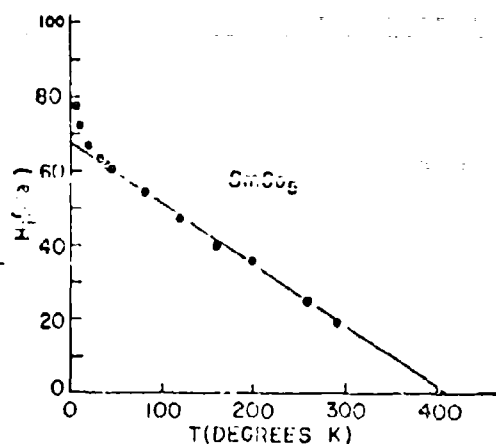
Figure 18. Room Temperature
Hysteresis Loops

Figure 19. Temperature Dependence of H_1

There is a relaxation associated with this effect which is strongly dependent on the internal field, $H_{int} = H-(4/3) \pi M$ where M is the bulk magnetization. $1/\tau$ (τ is the relaxation time) was measured as a function of H_{int} and is shown in Figure 20. The dashed line between the two points at $H_{int} = \pm 12.5$ Oe is an upper bound on $1/\tau$. In this region τ became very long and difficult to measure.
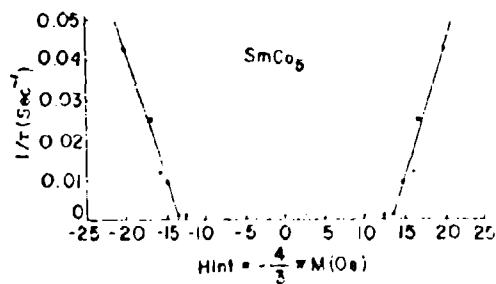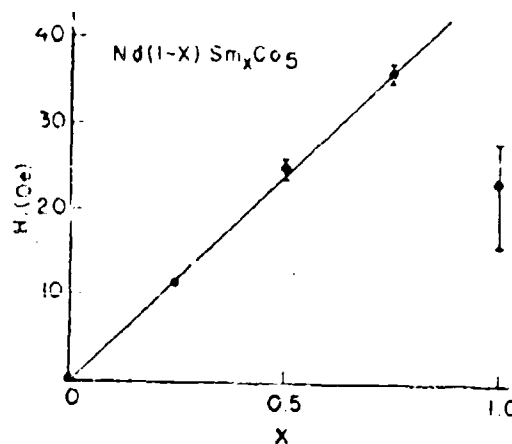

Figure 20. $1/\tau$ as a Function of H_{int}

Figure 21. Dependence of H_1 on x at Room Temperature

69

The dependence of H_i on x at room temperature for the mixed alloy $Nd(1-x)Sm_xCo_5$ is shown in Figure 21. The behavior in the region from x 0 to x .75 is expected since a nonzero H_i is associated with a material of high anisotropy and H_i should be proportional to the Sm concentration. An unexpected result appears as a sharp drop from the linear relation x = 1. The bars on the data represent the extreme range of values measured on several spheres with the same x, while the experimental points are the average of all the measurements. There is a strong indication that the magnitude of the fluctuations in H_i is also related to x.

The sharp departure of H_i from a linear relation was checked with other macroscopic properties such as the saturation magnitization, M_s and the anisotropy constant, K_1, but no correlation could be found since both M_s and K_1 were strictly linearly dependent on x.

10. 3 MODEL

The model shown in Figure 22 can correlate the experimental data. We will consider a portion of the domain wall, with sides of length 2a, as an individual unit interacting with one pinning site. The magnetic energy per unit, treating it as if it were uncoupled from the rest of the domain wall is,

$$E = -2M_sH_{int}x(2a)^2 = -8M_sH_{int}a^2x \qquad (1)$$

The statistical probability of a jump to the right, across a barrier of height E_A, per second is,

$$i/\tau = A\exp\left[\frac{-(E_A - 8M_sH_{int}a^2[x - a])}{kT}\right]$$

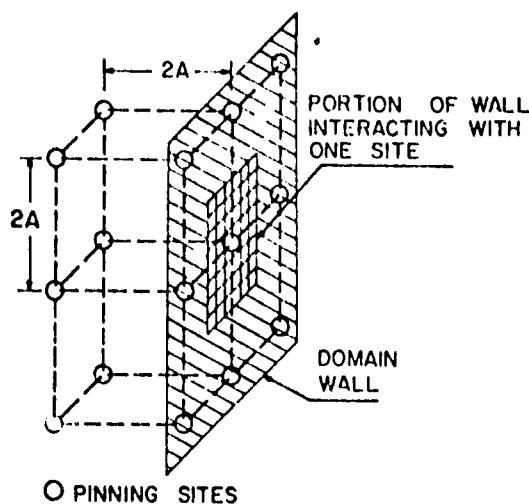$$A\exp\left[\frac{-E_A + 8M_sH_{int}a^3}{kT}\right] \qquad (2)$$

Figure 22. The Model

.We suggest that E_A is large enough so that $1/\tau \simeq 0$, on the time scale of our experiment, for small values of H_{int}. Then M will not change until $8M_s H_{int} a^3$ approaches the value E_A. This would make $1/\tau$ strongly dependent on H_{int} in qualitative agreement with the experimental results. In fact the hysteresis loop should turn the corner, at a constant sweep rate, when the exponent in Equation (2) is equal to a constant which we will somewhat arbitrarily, take to be -1, or,

$$8M_s a^3 H_i/k = E_A/k - T = T_c - T \qquad (3)$$

This equation predicts the observed linear relation between H_i and T. This also suggests that the initial τ, measured when $H_{int} = H_i$, should be independent of T. This effect was also verified within experimental error.

The second equation in this section predicts an exponential dependence of $1/\tau$ on H_{int}, whereas Figure 20 shows a much sharper break than exponential. One might expect this discrepancy to be removed if the coupling of the individual unit to the rest of the domain wall is considered. T_c can

71

be estimated from Equation (3) by setting $T = 0$ and substituting the extrapolated $T = 0$ values of $H_i = 67$ Oe, $M_s = 968$ emu/cc, and setting an equal to half a lattice spacing which yields $T_c = 0.06^\circ K$. Thus, one would expect the effect to thermally wash out. On the other hand if we use the experimental value of $T_c = 410^\circ K$ and solve for 2a we find,

$$2a = 2(T_c k/8M_s(0)H_i(0))^{1/3} = 97 \times 10^{-8} cm. \tag{4}$$

2a can also be determined independently by measuring the slope at the bottom or the top of the hysteresis loop, and using the standard relation for parallel domain walls,

$$2 x/W = X H/M_s \tag{5}$$

where x is the change in the position of a domain wall from equilibrium and X is the magnetic susceptibility. Use of the $T = 0$ values given above, $X = 2.69 \times 10^{-3}$ emu/cc/Oe, and $W = 59.5 \times 10^{-4}$ cm, the domain width adjusted for our samples size,(6) yields $2x = 2a = 114 \times 10^{-8}$ cm, in reasonable agreement with Equation (4).

A final check to see if the model was self consistent was obtained by solving the following equation for M.

$$dM/dt = (3H/4 \pi - M)/\tau. \tag{6}$$

Experimental values of τ from Figure 20 were used. The result is shown in Figure 23. It can be seen that the measured values of τ indicate that M should have sharper corners and approach an equilibrium situation faster than the measured curve does.

The period associated with the pinning sites is larger than the period of the lattice which implies the pinning sites are associated with imperfections which tend to be ordered. One would not expect perfect order and we suggest a nearly ordered array of imperfections with 2a fluctuating mildly as we
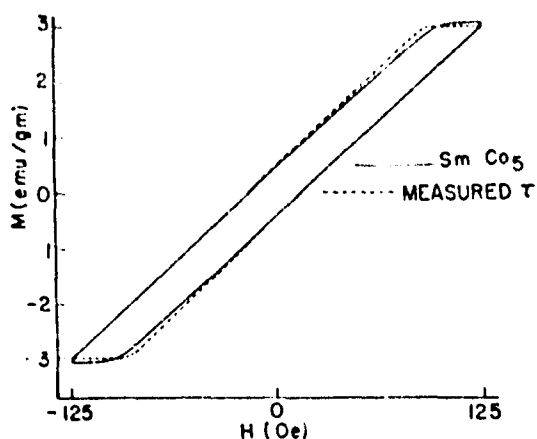
72

Figure 23. Comparison of the
Measured Hysteresis
Loop to one Calculated
From Measured τ's
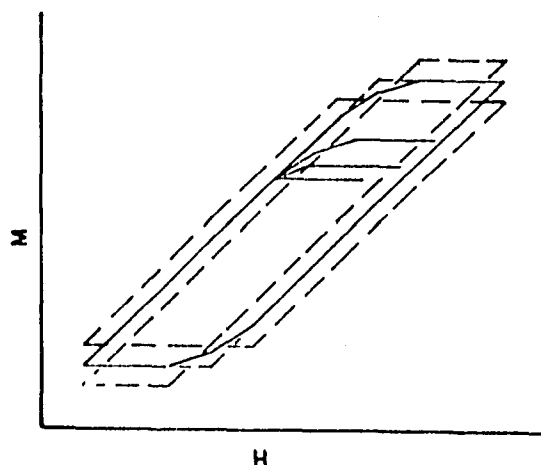
Figure 24. Expected Effects if 2a
Mildly Fluctuates with
Position in the Lattice

proceed through the lattice. The net effect would be a bulk hysteresis loop
which is a summation of individual sharp cornered loops with unique H_i's,
each one associated with portions of a domain wall encountering a region
with a unique well defined 2a. Some expected effects associated with this
interpretation are shown in Figure 24.

Firstly, it is evident that this interpretation can resolve the apparent
discrepancy between the calculated curve and the measured curve.
Secondly, we would expect a variation in the curve shapes from crystal to
crystal reflecting a variation in the degree of order. Extreme examples
of this are shown in Figures 25 and 26. Figure 25 would be associated with
a highly disordered array and is approaching normal minor loop behavior.
Figure 26 indicates a higher degree of order. Thirdly, we now proceed on
the left side of the loop to some point, designated by the intersection of
the short solid lines in Figure 24, then increase the field being careful
to stay away from behavior associated with the right side for any individual
loop. Now if the field is again decreased, while recording, the intrinsic
sharp corner should be revealed since all the individual loops turn the

73

corner at the same field as indicated by the short line. However, if we get close enough to the right side so that some smaller loops have begun to drift
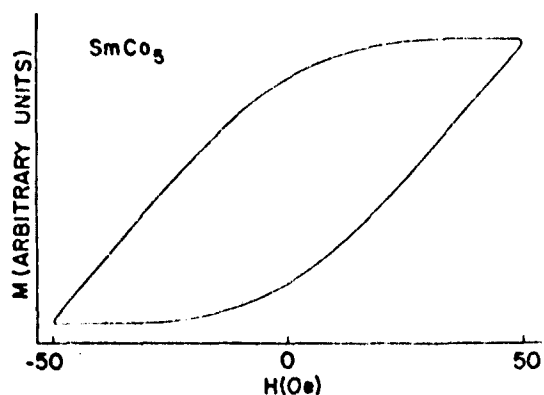

Figure 25. Hysteresis Loop Associated with a Highly Disordered Array of Imperfections
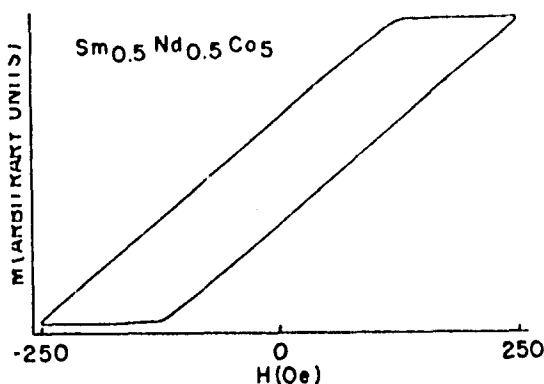
Figure 26. Hysteresis Loop Associated with a Nearly Order Array of Imperfections

up, then decrease the field, recording again, the corner will become rounder since some of the small loops will begin to drift down before the larger ones. This effect, as indicated by the longer lines in Figure 24, becomes stronger with closer approaches to the right side. Figure 27 shows this effect quite dramatically, finally making the model completely self consistent.
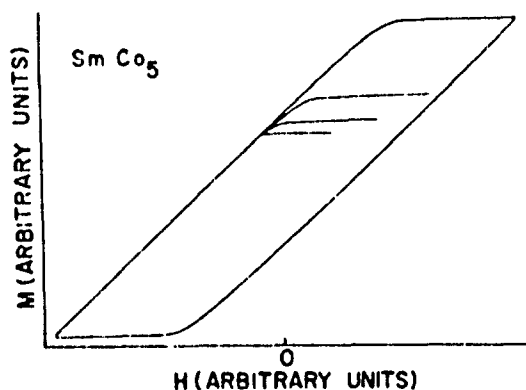

Figure 27. Experimental Observation of the Intrinsic Sharp Corner

10.4 DISCUSSION OF RESULTS

It is interesting to note that the temperature dependence of H_i, Figure 19, is very similar to that reported for H_c in small particles by Benz and Martin.[7] The magnitude of the effect is much smaller, however, and the

74

$H_i = 0$ intercept occurs at $T_c = 410^\circ K$ compared to $T_c = 700^\circ K$ for $H_c = 0$. The possibility that the pinning sites which lead to $H_i \neq 0$ are related to the pinning or nucleating sites on the surfaces of small particles will be explored in the future.

Finally, it should be mentioned that for a high energy domain wall arguments based on a small unit of the wall acting individually may lead to rather large errors. In fact, the large increase in wall energy that would be associated with one unit hopping may make a larger portion of the wall consisting of many coupled units hopping over their individual barriers a more probable event. This means that 2a may have been over estimated or $2a \lesssim 100 \times 10^{-8}$ cm.

REFERENCES FOR PART III

1. J. J. Becker, IEEE Trans. Magn. <u>Mag-7,</u> 644 (1971).

2. F. F. Westendorp, Appl. Phys. Lett. <u>20</u>, 441 (1972).

3. T. Egami and C. D. Graham, Jr. , JAP <u>42</u>, 1299 (1971).

4. K. N. R. Taylor, D. Melville, and G. J. Primaves, J. Phys F:Metal Phys. <u>2</u>, 584 (1972).

5. H. Zijlstra, JAP <u>41,</u> 4881 (1970).

6. J. D. Livingston and M. D. McConnel, JAP (In Press).

7. M. G. Benz and D. L. Martin, IEEE Trans. , MAG (In Press).